

J/ψ dissociation by light mesons in an extended Nambu Jona-Lasinio model

A. Bourque and C. Gale

*Department of Physics, McGill University
3660 University Street, Montreal, QC, Canada H3A 2T8*

(Dated: November 2, 2018)

A model for the dissociation of the J/ψ is proposed, where chiral symmetry is properly implemented. Abnormal parity interactions and mesonic form factors naturally arise from the underlying quark sub-structure. Analytic confinement of the light quarks is obtained through an appropriate choice of quark interaction kernels. Dissociation cross sections of the J/ψ by either a π or a ρ meson are then evaluated and discussed.

PACS numbers: 12.39.-x, 13.75.Lb, 11.30.Rd, 12.38.Mh

I. INTRODUCTION

Lattice simulations of quantum chromodynamics (QCD) predict a transition from hadronic matter to a plasma of quarks and gluons at a critical temperature of $T_c = 175 \pm 10$ MeV [1, 2]. To reproduce such a condition in a terrestrial environment, heavy ions are collided at relativistic energies. A typical space-time evolution involves the collision system going through various phases including possibly the elusive quark-gluon plasma (QGP). To find an unambiguous signature of this new state of matter proves challenging as other stages of the fireball expansion can also make contributions, which will thus constitute background.

One popular probe of the quark-gluon plasma is the charmonium yield modification first suggested by Matsui and Satz in a seminal paper [3]. In their original scenario, the charmonia produced in the earliest stage of the collision is expected to be suppressed by the QGP due to color screening [4]. But late stage hadronic dissociation could generally also occur, thus making the sources of the suppression difficult to disentangle: understanding the charmonium dissociation within a hadronic gas becomes essential. However, very little is known experimentally about these hadronic dissociation processes and one has to rely on theoretical calculations.

Most studies focus on dissociation channels of the charmonia by pions as it is the most abundant particle in the produced hadronic gas. Moreover, since, in a thermal gas at realistic temperature, the pions have just enough energy to dissociate the charmonium ground-state, the J/ψ , the cross section near threshold is of particular interest. Various approaches can be used including non-relativistic potential models [5, 6, 7, 8], QCD sum rules [9, 10, 11, 12, 13, 14, 15, 16], and constituent-quark based formalisms [17, 18, 19, 20, 21, 22, 23]. Alternatively, phenomenological Lagrangians can also be employed [24, 25, 26, 27, 28, 29]. However, the implementation of chiral symmetry has not uniformly been done in all Lagrangian models [30]. This could then have an important phenomenological consequence, as it is expected to soften the cross section near the production threshold.

In Ref. [31, 32], the effect of chiral symmetry on the dissociation cross sections was investigated within a chiral symmetric phenomenological Lagrangian approach. It was shown that for a certain class of interactions the dissociation transition amplitudes should vanish as the pion momentum goes to zero (soft-pion theorem). Although, a reduction was observed near threshold, the effect of introducing the so-called abnormal parity interactions was at least as important as that of the implementation of chiral symmetry. This observation could be traced back to the fact that these abnormal parity interactions circumvent the soft-pion theorem. The results of Ref. [32], in particular the overall magnitude of the calculate cross sections, depended heavily on the parameterization of the ad-hoc form factors. It is the purpose of this article to address this issue by proposing a chiral-symmetric model of the J/ψ -dissociation whereby the form factors naturally arise from the underlying quark structure. This constituent-quark framework builds on models presented in Refs. [17, 18, 19, 20, 21, 22, 23]. However, strictly speaking, the model presented here is an extension to the charm sector of Refs. [33, 34, 35] which itself is a generalisation of the Nambu Jona-Lasinio (NJL) model [36, 37] where the four-point interaction kernels are non-local and chiral symmetry is implemented at the quark level. Within this formalism, the mesonic form factors can then be calculated, and by choosing the appropriate light-quark kernels, it is possible to push to higher energies, or even remove, the unphysical production threshold of the ρ meson into the continuum (i.e, into a $\bar{q} - q$ pair) which at zero temperature and density should not occur. This then also permits the calculation of the ρ -induced J/ψ dissociation which is used to assess the effect of light resonances on the overall dissociation strength.

This article is organized as follows: after introducing the quark interaction kernels and considering their properties, quark propagators are discussed with an emphasis on ways of generating quark confinement. Meson bound states are then found along with meson-quark vertex functions. Three- and four-point meson interactions mediated through quark loops are written down. Finally, after fixing the various parameters using a combination of lattice results and

empirical information, the behaviors of meson propagators, vertices, and cross sections are examined. The analytic continuation prescriptions are detailed in Appendix A. In Appendix B, the isovector axial Ward identity is explicitly checked, while in Appendix C decay processes used to fix the parameters are evaluated. Finally, the amplitudes of the various dissociation channels studied here can be found in Appendix D.

II. QUARK INTERACTION KERNELS

In this model, chiral symmetry is implemented at the quark level. As in Ref. [32], the mesonic content includes the π , ρ , J/ψ , D , D^* , and the chiral partners of the open charmed mesons, namely D_0^* and D_1 mesons, in order to describe the dissociation processes of interest. Besides these, the σ and a_1 mesons will also naturally appear in such an approach due to chiral symmetry. However, as for the NJL model, only global color invariance is introduced allowing to account for the number of quark colors, N_c , in QCD. Moreover, only color singlets are written down.

With this in mind, the minimal action is

$$\mathcal{S} = \int dx \{ \bar{q}(x) (i\partial - m_c^q) q(x) + \bar{Q}(x) (i\partial - m_c^Q) Q(x) \} + S_{int} \quad (1)$$

where q and Q are the fermion fields for the light and heavy quarks, respectively, and the interactions are decomposed into

$$S_{int} = \mathcal{S}_{int}^{qq} + \mathcal{S}_{int}^{qQ} + \mathcal{S}_{int}^{QQ} \quad (2)$$

with

$$\mathcal{S}_{int}^{f_1 f_2} = \left[\prod_{k=1}^4 \int dx_k \right] K_{abcd}^{f_1 f_2}(x_1, x_2, x_3, x_4) \bar{\psi}_{f_1}^a(x_1) \psi_{f_1}^b(x_2) \bar{\psi}_{f_1}^c(x_3) \psi_{f_2}^d(x_4). \quad (3)$$

The kernels, K , can be further decomposed into

$$K_{abcd}^{f_1 f_2}(x_1, x_2, x_3, x_4) = \sum_i H_i^{f_1 f_2}(x_1, x_2, x_3, x_4) \left(\bar{\Gamma}_{ab;i}^{f_1 f_2} \otimes \Gamma_{cd;i}^{f_1 f_2} \right) \quad (4)$$

where the H_i parametrise the strengths and the profiles of the non-local interactions and f_i labels the flavor (either q or Q), $\tilde{\Gamma} = \gamma_0 \Gamma^\dagger \gamma_0$. The Dirac and flavor structures for the present model are then

$$\begin{aligned} \Gamma_{\{S,P,V,A\}}^{qq} &= \{1, i\gamma_5 \tau^a, \gamma_\mu \tau^a, \gamma_\mu \gamma_5 \tau^a\}, \\ \Gamma_{\{S,P,V,A\}}^{qQ} &= \{1, i\gamma_5, \gamma_\mu, \gamma_\mu \gamma_5\}, \\ \Gamma_V^{QQ} &= \gamma_\mu. \end{aligned} \quad (5)$$

Chiral symmetry then imposes that $H_S^{\{qq,qQ\}} = H_P^{\{qq,qQ\}}$ and $H_V^{\{qq,qQ\}} = H_A^{\{qq,qQ\}}$. This choice can be explicitly checked by using the global transformation for the light quark field [32] and remembering that the heavy quark field is invariant under this symmetry.

The most general form of H_s is constrained by translational invariance. To make this property explicit a change of variables as in Ref. [38] is made, namely

$$\begin{aligned} X &= \frac{1}{2} (-x_1 - x_2 + x_3 + x_4) \quad , \quad X' = \frac{1}{4} (x_1 + x_2 + x_3 + x_4) \quad , \\ x &= x_2 - x_1 \quad , \quad x' = x_4 - x_3. \end{aligned} \quad (6)$$

With these and suppressing all indices, the kernels become

$$\begin{aligned} H_i^{f_1 f_2}(x_1, x_2, x_3, x_4) &= \prod_k \int dp_k e^{-i \sum_j x_j \cdot p_j} H_i^{f_1 f_2}(p_1, p_2, p_3, p_4) \\ &= \prod_k \int dp_k e^{i(p_1 - p_2) \cdot \frac{x}{2}} e^{i(p_3 - p_4) \cdot \frac{x'}{2}} e^{i(p_1 + p_2 - p_3 - p_4) \cdot \frac{X}{2}} \\ &\times e^{-i(p_1 + p_2 + p_3 + p_4) \cdot X'} H_i^{f_1 f_2}(p_1, p_2, p_3, p_4) \end{aligned} \quad (7)$$

where the momenta are taken to be in-going. Translation invariance then amounts to requiring that under an arbitrary shift by a four vector a , the kernels respect

$$H_i^{f_1 f_2}(x_1 + a, x_2 + a, x_3 + a, x_4 + a) = H_i^{f_1 f_2}(x_1, x_2, x_3, x_4), \quad (8)$$

or more specifically that the H_i do not depend on X' . This then restricts their form in momentum-space to

$$\tilde{H}_i^{f_1 f_2}(p_1, p_2, p_3, p_4) = (2\pi)^4 \delta^{(4)}(P') \tilde{H}_i^{f_1 f_2}(p', p, P) \quad (9)$$

where we have defined

$$\begin{aligned} P &= \frac{1}{2}(p_1 + p_2 - p_3 - p_4) \quad , \quad P' = (p_1 + p_2 + p_3 + p_4) \\ p &= \frac{1}{2}(p_1 - p_2) \quad , \quad p' = \frac{1}{2}(p_3 - p_4). \end{aligned} \quad (10)$$

The original NJL model is given by

$$\tilde{H}_i^{f_1 f_2}(p_1, p_2, p_3, p_4) = G_i^{f_1 f_2} (2\pi)^4 \delta^{(4)}(P') \quad (11)$$

where the $G_i^{f_1 f_2}$ are the interaction strengths, which have a dimension of inversed energy squared. Here, we will consider a fully-separable interaction in momentum-space inspired by an instanton-based approach [34], i.e.,

$$\tilde{H}_i^{f_1 f_2}(p_1, p_2, p_3, p_4) = \frac{1}{2}(2\pi)^4 G_i^{f_1 f_2} \delta(P') f_{f_1}(p_1) f_{f_1}(p_2) f_{f_2}(p_3) f_{f_2}(p_4) \quad (12)$$

where $f(p_i)$ are the quark form factors modeling the non-locality of the interactions. These are normalised to one at zero impulse and their specific forms will be chosen, in the light sector, to provide confinement. Moreover, they act as UV regulators for the loop integrals removing the need for a UV cutoff as in the original NJL model. The G_i constants scale like $1/N_c$, which can be inferred by considering the simplest four-point interaction in QCD : the one-gluon exchange interaction between four quarks. The $1/N_c$ scaling of the four-point vertex will be used in what follows to determine an approximation scheme consistent with chiral symmetry. This particular choice of kernels also greatly simplifies the search for mesonic bound states and facilitates numerical integration.

III. QUARK PROPAGATORS

A. Light quark sector

The general solution of the Schwinger-Dyson equation (SDE) in momentum-space is given by [40]:

$$S_q(p) = Z_q(p) \frac{\not{p} - m_q(p)}{p^2 - m_q^2(p)} \quad (13)$$

where m_q and Z_q are the momentum-dependent mass function and wavefunction renormalization respectively.

Working in the mean field approximation or equivalently at leading order in $1/N_c$, the light quark propagator for the action of Eq. (3) reduces to [34, 39]

$$S_q(p) = \frac{1}{\not{p} - m_q(p)} \quad (14)$$

where the dynamical mass is given by

$$m_q(p) = m_c^q + iG_S f_q^2(p) \int \frac{d^4 k}{(2\pi)^4} f_q^2(k) \text{Tr} \{S_q(k)\}. \quad (15)$$

We note that only the scalar channel gives a non-zero contribution and the dynamical mass scales like N_C^0 as in QCD [39]. The above gap equation then admits the solution [34]

$$m_q(p) = m_c^q + (m_q(0) - m_c^q) f_q^2(p) \quad (16)$$

where $m_q(0)$ is the dynamical mass at zero momentum. The quark propagator can also be directly linked to the quark condensate in the chiral limit through the expression

$$\langle \bar{q}q \rangle_0 = -i \int \frac{d^4 k}{(2\pi)^4} \text{Tr} [S_q(k)]. \quad (17)$$

From the quark propagator it can be readily inferred that there will be no poles on the real axis in two cases: either the poles are complex [19] or there are no poles at all in the complex plane [42]. Here, we will consider the second case. However, to illustrate how this property is manifest we need to analytically continue the quark propagator to Euclidean space, i.e., the denominator becomes $p_E^2 + m^2(p)$.

We then follow Ref. [42] where the inverse of the quark propagator denominator, in the chiral limit, is parametrized as

$$\frac{1}{p^2 + m_q^2(p)} = \frac{1 - e^{-\mu p^2}}{p^2}. \quad (18)$$

Alternatives also exist such as the one found in Ref. [43]. Various limits can then be considered. For large positive p^2 , this quantity behaves as expected perturbatively, i.e., $1/p^2$. This is not the case for large *negative* p^2 where it diverges. This is not a major problem provided the mass function is probed only for small negative p^2 , i.e., small time-like separation in Minkowski space. As the infrared limit is approach, i.e., $p^2 \rightarrow 0$, the inverse quark propagator becomes constant and equal to μ . The cutoff parameter is then seen to be equal to $\mu = 1/m^2(0)$. This is sufficient to show that no poles exist. Mathematically, this function property is called entire, and this realization of quark confinement is deemed analytic. Reinstating the current quark mass yields

$$m_q(p) = \sqrt{\frac{m_c^{q2} + p^2 e^{-\mu(p^2 + m_c^{q2})}}{1 - e^{-\mu(p^2 + m_c^{q2})}}} \quad (19)$$

where the principal branch has been chosen.¹ In what follows, we will refer to the model using this functional form for the dynamical mass as Model I (MI). This choice will complicate the evaluation of n -point functions as branch cuts will generally appear. Since the zero-momentum light-quark mass should be of the order of a few hundred MeVs [7, 22], the parameter μ will be greater than one. Therefore, for $p^2 > 0$, the dynamical mass will exhibit a steep decrease. To control this ultraviolet behavior, we also consider an alternative dynamical mass model (MII), which is constructed by substituting $m_c^q \rightarrow m_c^q + (m_0 - m_c^q)e^{-\alpha p^2}$ in Eq. (19) where m_0 and α are two additional parameters. The steep decline for $p^2 > 0$ can then be overcome.

B. Heavy quark sector

For the heavy flavor sector, again no wavefunction renormalization is possible for this model at leading order in $1/N_c$. Furthermore, there is no heavy quark scalar interaction in the quark action. Therefore, there is no dynamical mass generation at the mean field level contrary to the light quark sector. This leaves the charm quark form factor unspecified. Here, we will chose:

$$f_Q(p) = e^{-\beta_Q p^2} \quad (20)$$

in Euclidean space where β_Q will be fixed by considering the decay of the J/ψ into dileptons (see Appendix C).

IV. MESON BOUND STATES

A. Meson-quark vertex functions and meson propagators

Interactions amongst constituents lead to the emergence of bound states provided attractive channels exist between them. In QCD, these occur, at least perturbatively, in the singlet-color channel between a quark and anti-quark. At

¹ This choice, through Eq.(16), leads to an action that is not linear in the current mass, contrary to the QCD action, and results from enforcing analytic confinement in this particular model. However, it can be shown that the GMOR relation holds to first order in m_c for such a mass model (see Ref.[42]).

all orders in quantum field theory, bound states are found by considering the pole structure of the scattering matrix, S . Following Refs. [44, 45], the inhomogeneous Bethe-Salpeter equation (BSE) satisfied by the T -matrix for a given flavor content, i.e., the interacting part of the scattering matrix, is

$$T(p, p', P) = K(p, p', P) + \int dp'' K(p, p'', P) S(p_-) T(p'', p', P) S(p_+) \quad (21)$$

where the Dirac indices and flavor labels have been suppressed for clarity and $p_{\pm} = p'' \pm \frac{1}{2}P$.

To solve the BSE, we have to specify, besides the quark propagators, the scattering kernels. In general, since they comprise of an infinite sum of diagrams, a truncation scheme must be implemented. If the Hartree propagator for light quark is used and we require chiral symmetry to be maintained, then the scattering kernels involving light quarks are uniquely determined: they cannot contain exchange terms and their functional forms are fixed to that of Eq. (12). This is known in low-energy nuclear physics as the random-phase approximation (RPA) and is the counterpart of the mean field hypothesis for solving the SDE. Moreover, without any surprises, their N_C -scaling is that of the G_i couplings. The kernels being fully separable, the BSE admits the solution

$$T^{f_1 f_2}(p, p', P) = f_{f_1}(p_1) f_{f_1}(p_2) f_{f_2}(p_3) f_{f_2}(p_4) \hat{T}^{f_1 f_2}(P) \quad (22)$$

where momentum conservation is implicit and $\hat{T}^{f_1 f_2}(P)$ are the T -matrix with the $f(p)$ factored out.

Next following Ref. [46], the BSE is decomposed into independent Dirac channels. This can be achieved by using the projection operators

$$T_{\mu\nu} = g_{\mu\nu} - \hat{P}_\mu \hat{P}_\nu, \quad L_{\mu\nu} = \hat{P}_\mu \hat{P}_\nu \quad (23)$$

where $\hat{P}_\mu = P_\mu / \sqrt{P^2}$. The scattering kernels can then be re-arranged for the pseudo-scalar and scalar channels as

$$\hat{K}_{\{S,P\}}^{f_1 f_2} = G_{\{S,P\}}^{f_1 f_2} \left(\tilde{\Gamma}_{\{S,P\}}^{f_1 f_2} \otimes \Gamma_{\{S,P\}}^{f_1 f_2} \right) + G_{\{V,A\}}^{f_1 f_2} \left(\tilde{\Gamma}_{\{V,A\}}^{f_1 f_2;L} \otimes \Gamma_{\{V,A\}}^{f_1 f_2;L} \right) \quad (24)$$

and

$$\hat{K}_{\{V,A\}}^{f_1 f_2} = G_{\{V,A\}}^{f_1 f_2} \left(\tilde{\Gamma}_{\{V,A\}}^{f_1 f_2;T} \otimes \Gamma_{\{V,A\}}^{f_1 f_2;T} \right) \quad (25)$$

for the vector and axial ones where

$$\Gamma_{\{V,A\}}^\mu = (T_\nu^\mu + L_\nu^\mu) \Gamma_{\{V,A\}}^\nu = \Gamma_{\{V,A\}}^{T\mu} + \Gamma_{\{V,A\}}^{L\mu}. \quad (26)$$

Note also that the left- and right-hand parts of a given flavor and Dirac matrix product is associated with the in- and out-going quark states, respectively. Thus the kernels should be read from left to right. Similarly, the \hat{T} -matrix can be decomposed into products of Lorentz covariant tensors giving

$$\begin{aligned} \hat{T}_{\{S,P\}}^{f_1 f_2} &= M_{\{SS,PP\}}^{f_1 f_2} \left(\tilde{\Gamma}_{\{S,P\}}^{f_1 f_2} \otimes \Gamma_{\{S,P\}}^{f_1 f_2} \right) + M_{\{SV,PA\}}^{f_1 f_2} \left(\tilde{\Gamma}_{\{S,P\}}^{f_1 f_2} \otimes \Gamma_{\{V,A\}}^{f_1 f_2;L} \right) \\ &+ M_{\{VS,AP\}}^{f_1 f_2} \left(\tilde{\Gamma}_{\{V,A\}}^{f_1 f_2;L} \otimes \Gamma_{\{S,P\}}^{f_1 f_2} \right) + M_{\{VV,AA\}}^{f_1 f_2;L} \left(\tilde{\Gamma}_{\{V,A\}}^{f_1 f_2;L} \otimes \Gamma_{\{V,A\}}^{f_1 f_2;L} \right), \end{aligned} \quad (27)$$

and

$$\hat{T}_{\{V,A\}}^{f_1 f_2} = M_{\{VV,AA\}}^{f_1 f_2;T} \left(\tilde{\Gamma}_{\{V,A\}}^{f_1 f_2;T} \otimes \Gamma_{\{V,A\}}^{f_1 f_2;T} \right) \quad (28)$$

where the M components are functions of P^2 . It is clear that, in general, mixing occurs between channels, i.e., the longitudinal component of the vector and axial channels contribute to the scalar and pseudo-scalar ones respectively, and that the T -matrix is then block-diagonal. From the BSE, it is then seen that for a given flavor and Dirac channels, a given M matrix satisfies the equation

$$M = G [1 + JM] = \frac{G}{1 - GJ} \quad (29)$$

where all labels have been suppressed. The fermion-loop matrix is then given by

$$iJ_{ij}^{f_1 f_2}(P^2) = - \int dk f_{f_1}^2(k_-) f_{f_2}^2(k_+) \text{Tr} \left[\Gamma_i^{f_1 f_2} S_{f_1}(k_-) \tilde{\Gamma}_j^{f_1 f_2} S_{f_2}(k_+) \right] \quad (30)$$

where the minus sign on LHS is due the normal ordering of fermion fields, $k_{\pm} = k \pm \frac{P}{2}$, and the matrix indices are i and j .² This equation shows that a pole will develop in the T -matrix when

$$\Delta = |1 - GJ(m_M^2)| = 0 \quad (31)$$

where m_M is the mass of the meson. On one hand, near this point, the T -matrix admits the solution

$$T(p, p', P) \approx \frac{i\bar{\chi}_M(p, P) \otimes i\chi_M(p', P)}{P^2 - m_M^2} \quad (32)$$

where the wavefunction for meson M is defined as

$$\chi_M(p', P) = \langle \bar{q}_{f_1} q_{f_2} | M(P) \rangle = g_M f_{f_1}(p_1) f_{f_2}(p_2) \left(1 - \frac{a_M}{m_M} \hat{P} \right) \Gamma_M^{f_1 f_2} \quad (33)$$

with $p' = \frac{1}{2}(p_3 - p_4)$. The coupling and mixing parameters are found by solving Eq. (29) using Eq.(32) yielding for a meson of spin s : $g_m = (-1)^s M^{00}/d\Delta/dP^2$ and $a_m = M^{11}/M^{00}$. Note that for channels where there is no mixing $a_M = 0$. On the other hand, for P^2 far from the on-shell condition, the \hat{T} -matrix can be written as

$$\hat{T}_M = ig_M \hat{\Gamma}_M^i \otimes ig_M \hat{\Gamma}_M^j \mathcal{D}_M(P^2) \quad (34)$$

where $\hat{\Gamma}_M^i = (1, \hat{P}) \otimes \Gamma_M^{f_1 f_2}$ and with the meson propagator given by

$$\mathcal{D}_M(P) = -\frac{1}{g_M^2} M_M(P) \quad (35)$$

where the tensorial structure is suppressed.

B. Meson interactions

Having discussed the couplings between quarks and mesons, the interactions amongst the mesons are now examined. As for the meson self-energies, only interactions mediated by quarks will be studied; mesonic fluctuations being sub-leading in a $1/N_c$ expansion.

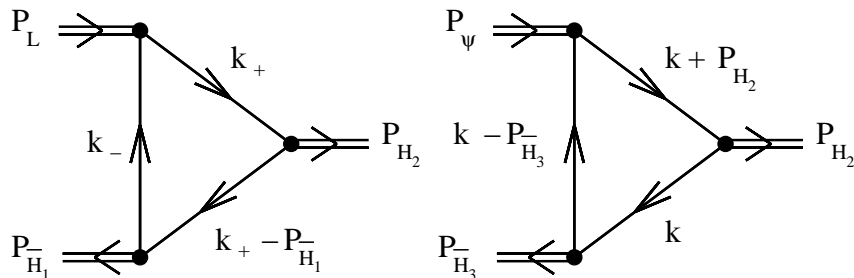


FIG. 1: Momentum conventions for the three-point vertex functions.

To evaluate the dissociation cross sections, the three- and four-point interactions have to be written down. The former are further divided into two, namely interactions between one light meson, either the pion or the ρ meson and two open charmed mesons; or interactions between the J/ψ and two open charmed mesons. The momentum flows for these two cases are depicted in Fig. 1. Here, in general, one of the three mesons will be off-shell and the kinematical

² The analytic continuation for these two-loop integrals is explained in Appendix A.

variable t is then the associated momentum transfer. The expressions for the meson form factors are

$$iF_{L\bar{H}_1(H_2)}^i(t) = - \int dk \text{Tr} \left[i\chi_L iS_q(k_-) ig_{H_2} \hat{\Gamma}_{H_2}^i iS_Q(k_+ - P_{\bar{H}_1}) i\bar{\chi}_{\bar{H}_1} iS_q(k_+) \right], \quad (36)$$

$$iF_{LH_2(\bar{H}_1)}^i(t) = - \int dk \text{Tr} \left[i\chi_L iS_q(k_-) i\bar{\chi}_{H_2} iS_Q(k_+ - P_{\bar{H}_1}) ig_{H_1} \hat{\Gamma}_{\bar{H}_1} iS_q(k_+) \right] \quad (37)$$

and

$$iF_{\psi H_2(\bar{H}_3)}^i(t) = - \int dk \text{Tr} \left[i\chi_\psi iS_Q(k - P_{\bar{H}_3}) ig_{H_3} \hat{\Gamma}_{H_3}^i iS_q(k) i\bar{\chi}_{H_2} iS_Q(k + P_{H_2}) \right] \quad (38)$$

$$iF_{\psi \bar{H}_3(H_2)}^i(t) = - \int dk \text{Tr} \left[i\chi_\psi iS_Q(k - P_{\bar{H}_3}) i\bar{\chi}_{\bar{H}_3} iS_q(k) ig_{H_2} \hat{\Gamma}_{H_2}^i iS_Q(k + P_{H_2}) \right] \quad (39)$$

where the momentum arguments of the wavefunctions have been suppressed for clarity, L and H label the light and open charmed mesons respectively, the minus sign is due to the fermion-loop, and the round parentheses indicate which meson is off-shell. The extra label i notes that the form factor can be a two-component vector due to mixing.

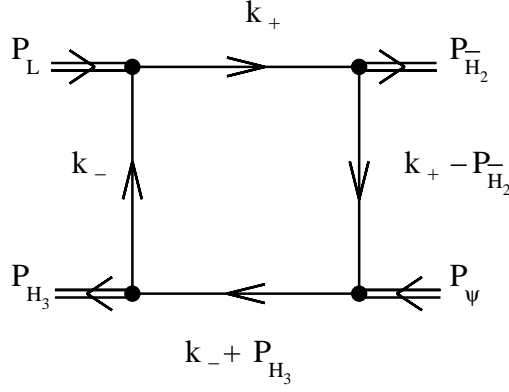


FIG. 2: Momentum convention for the four-point vertex functions.

Similarly, the general expression for the four-point interaction, illustrated in Fig. 2, is given by

$$iF_{L\psi\bar{H}_2H_3}(s, t) = - \int dk \text{Tr} \left[\begin{aligned} & i \chi_L iS_q(k_-) i\bar{\chi}_{H_3} iS_Q(k_- + P_{H_3}) i\chi_\psi \\ & i S_Q(k_+ - P_{\bar{H}_2}) i\bar{\chi}_{\bar{H}_2} iS_q(k_+) \end{aligned} \right] \quad (40)$$

where again the minus sign is due to the fermion-loop. The analytic continuation of the loop integrals is discussed in Appendix A.

V. RESULTS

A. Parameter fixing

The isospin-averaged masses of the pion, ρ , D , D^* , and J/ψ mesons used in what follows are 0.138 GeV, 0.770 GeV, 1.868 GeV, 2.009 GeV, and 3.096 GeV respectively. The first model (referred as MI) is that of Eq. (19) and has four parameters, namely m_c^Q , β_Q , μ , and m_c^q . Three observables, i.e, the pion decay constant [Eq. (C21)], the dielectron decay width of the J/ψ meson [Eq. (C6)], and the the decay width of the D^* into $D-\pi$ final state [Eq. (C3)], can be then used to partly constrain the possible parameter values. Specifically, m_c^q is determined in order to reproduce the

pion decay constant value since its expression [Eq. (C21)] has a strong m_c^q -dependence. While, for a fixed m_c^Q , the range parameter, β_Q , is constrained by the experimental dielectron decay width of the J/ψ [Eq.(C6)]. This leaves the open charmed decay constant [Eq. (C3)] to fix both m_c^Q and μ . To restrict the possible solutions, we also required that the light-quark dynamical mass at zero-momentum be of the order of a few hundred MeVs as it is seen from lattice results [38] and as used in other phenomenological studies [7, 22]. We further require that m_c^Q obey the constraint $m_{J/\psi} < 2m_c^Q$ since the model is non-confining in the heavy sector. With these additional constraints, one possible set of values is $m_c^Q = 1.59 \text{ GeV}$, $\beta_Q = 0.06 \text{ GeV}^{-2}$, $m_c^q = 12 \text{ MeV}$, and $\mu = 8 \text{ GeV}^{-2}$. These then yield $f_\pi = 94.78 \text{ MeV}$, $\Gamma_{J/\psi \rightarrow e^+e^-} = 5.44 \text{ keV}$, and $g_{\pi DD^*} = 18.62$ which are to be compared to the experimental values of $f_\pi = 93 \text{ MeV}$, $\Gamma_{J/\psi \rightarrow e^+e^-} = 5.5 \pm 0.14 \pm 0.02 \text{ keV}$ [49], and $g_{\pi DD^*}^{\text{exp}} = 17.9 \pm 0.3 \pm 1.9$ [48]. The resulting light-quark mass at zero momentum is then $m_q(0) = 0.354 \text{ GeV}$, while the quark condensate is $-(237)^3 \text{ MeV}^3$ as calculated using Eq. (17). Both these values are slightly higher than those found in Ref. [34].

Introducing the substitution discussed earlier in Section III A into the Eq. (19), the number of parameters in the light sector increases by two (model MII). Additional information is thus needed. An alternative could be to calculate other observables such as the ρ decay into two pions in order to fix the extra parameters. Rather, here a parametrisation of lattice data is used.³ Specifically, we will utilize the one proposed in Ref. [38], namely

$$m_q(p) = \alpha_m \left(\frac{\Lambda_m^2}{\Lambda_m^2 + p^2} \right)^{\frac{3}{2}} \quad (41)$$

where $\alpha_m = 0.343 \text{ GeV}$ and $\Lambda_m = 0.767 \text{ GeV}$. Fitting our model [Eq. (19)] to this parametrisation for $p^2 \in [0, 1]$ gives $m_0 = 0.227 \text{ GeV}$, $\alpha = 1.096 \text{ GeV}^{-2}$ and $\mu = 11.786 \text{ GeV}^{-2}$. The light current mass is then taken to be $m_c^q = 5.5 \text{ MeV}$ yielding $f_\pi = 92.11 \text{ MeV}$. The zero-momentum dynamical mass is then 0.331 GeV , while the quark condensate is now $-(239)^3 \text{ MeV}^3$. With the same values for the heavy-sector parameters, the coupling constant $g_{\pi DD^*}$ is 18.35 which is a prediction of the model and well within the experimental tolerance [48].

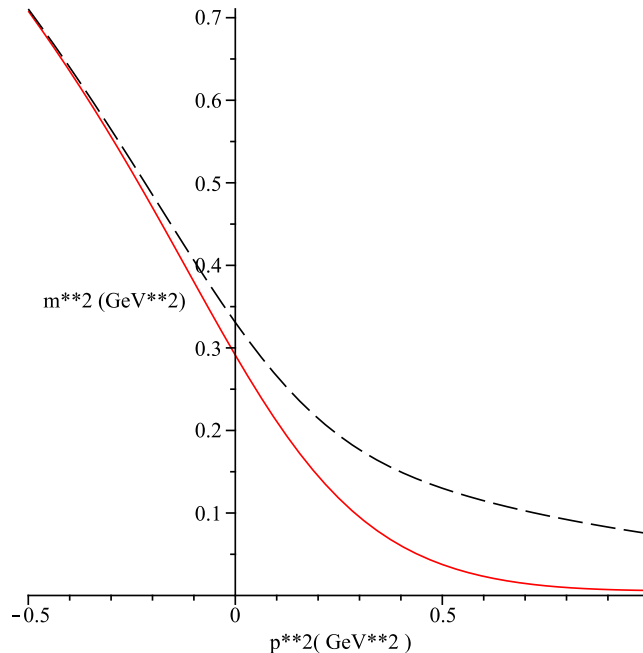


FIG. 3: (Color online) Light-quark dynamical mass models with $u = p^2$. The solid and dashed lines are the MI and MII models respectively.

Fig. 3 shows a comparison between the two light-quark mass models discussed. As seen, for $p^2 \leq 0$, the two models are very similar. The main difference is for $p^2 > 0$ where for MI the dynamical mass drops very quickly down

³ The quark mass is not a gauge-invariant quantity and thus dependent on the gauge chosen to carry out the simulation. The purpose here is to capture some flavor of the QCD dynamics.

to its asymptotic value of m_c^q . Both models have similar zero-momentum mass, quark condensate, and calculated observables. The only noted difference is in the light-quark current mass for which there is more than a factor two difference between models. Although the current mass for MII is within the range given by PDG [49], i.e., 1.3 to 5 MeV for the u -quark and of 3 to 7 MeV for the d -quark, one could wonder if introducing two extra parameters, m_0 and α , in order to reduce the current quark mass value is justified. At this point, we will retain the two models to ascertain if any other differences occur for vertices and cross sections.

With the parameters for MI and MII, the four-quark couplings, the meson-quark couplings, and the mixing coefficients can be evaluated. Their values are listed in Table I. Since the D_0^* and D_1 are the chiral partners of the D and D^* respectively, the masses are not independent and have to be calculated by finding the zeros of the respective meson propagator denominators. Doing so yields $m_{D_0^*} = 2.064$ GeV and $m_{D_1} = 2.249$ GeV, and, $m_{D_0^*} = 2.045$ GeV and $m_{D_1} = 2.231$ GeV for MI and MII, respectively. These are to be compared to the experimental masses of $m_{D_0^*} = 2.40$ GeV and $m_{D_1} = 2.43$ GeV. It is quite clear that neither model is capable of reproducing the absolute masses and the mass difference, i.e., $\Delta m_{exp} = 0.03$ GeV. This problem then implies that the interaction kernels or, in non-relativistic terms the potentials, require further modeling. This is left for a future study.

G_M	MI	MII	g_M	MI	MII
$G_{J/\psi}$	-1.145	-1.145	$g_{J/\psi}$	1.717	1.717
G_{D^*}	-6.690	-5.257	g_{D^*}	2.025	1.842
G_{D_1}	-6.690	-5.257	g_{D_1}	1.955	1.772
G_D	17.661	11.977	$g_D(a_D)$	4.667(0.301)	4.166(0.315)
$G_{D_0^*}$	17.661	11.977	$g_{D_0^*}(a_{D_0^*})$	3.654(0.166)	3.828(0.205)
G_ρ	-7.070	-6.147	g_ρ	1.336	1.219
G_π	52.562	31.052	$g_\pi(a_\pi)$	3.768(0.0220)	3.615(0.0233)

TABLE I: Quark-quark couplings, meson-quark couplings, and mixing coefficients.

B. Meson propagators and vertices

Having fixed the parameters for the two models, the meson propagators and vertices can now be examined. For the meson propagators, \mathcal{D}_M , as can be seen from Eq. (29), the asymptotic behavior is controlled by the two-point functions, J_M , as the quark-quark coupling, G_M , is independent of momentum.⁴ As $t \rightarrow \infty$, $J_M \rightarrow \infty$ and $\mathcal{D}_M \rightarrow 0$, while for $t \rightarrow -\infty$, $J_M \rightarrow 0$ and $\mathcal{D}_M \rightarrow -\frac{G_M}{g_M^2}$. Near the meson pole, the scalar part of the corresponding propagator [Eq. (32)] is expected to behave as

$$\mathcal{D}_M^{\text{pole}}(t) \propto \frac{(-1)^s}{t - m_M^2} \quad (42)$$

where s is the meson spin. Note that this form is used for the phenomenological Lagrangian studies of Refs [24, 25, 26, 27, 28, 29, 32].

Fig. 4⁵ illustrates the behaviors of the D^* and ρ propagators for MI and MII compared to that of Eq. (42). It is quite clear that the phenomenological propagators are comparable to the NJL ones only near the poles, and that the differences between the propagators of MI and MII are not significant. Although not shown on the figure, this latter observation holds true for $t > m_M^2$. Note that for $t \rightarrow -\infty$ the NJL-propagators exhibit the expected asymptotic behavior, i.e., it is non-zero as for the Lagrangian one, but rather $-\frac{G_M}{g_M^2}$.

Fig. 5 shows examples of three-point meson vertices. The curves labeled Lagrangian are the ad-hoc form factors multiplied by the relevant meson couplings used in Ref. [32]. Let us first consider the differences between the Lagrangian and the NJL approaches. We note that a relative agreement only exists for the coefficient of $F_{\pi\bar{D}(D^*)}$ proportional to pion momentum, while the overall magnitude of the coefficient proportional to the ρ -meson momentum

⁴ For simplicity, mixing is ignored here. Adding it does not alter the conclusions.

⁵ A logarithmic scale was used in order to permit the discrimination between the three curves. At the pole, the divergence should be infinite and the appearance of the contrary is just an artifact of the finite number of points in the numerical evaluation of the propagator.

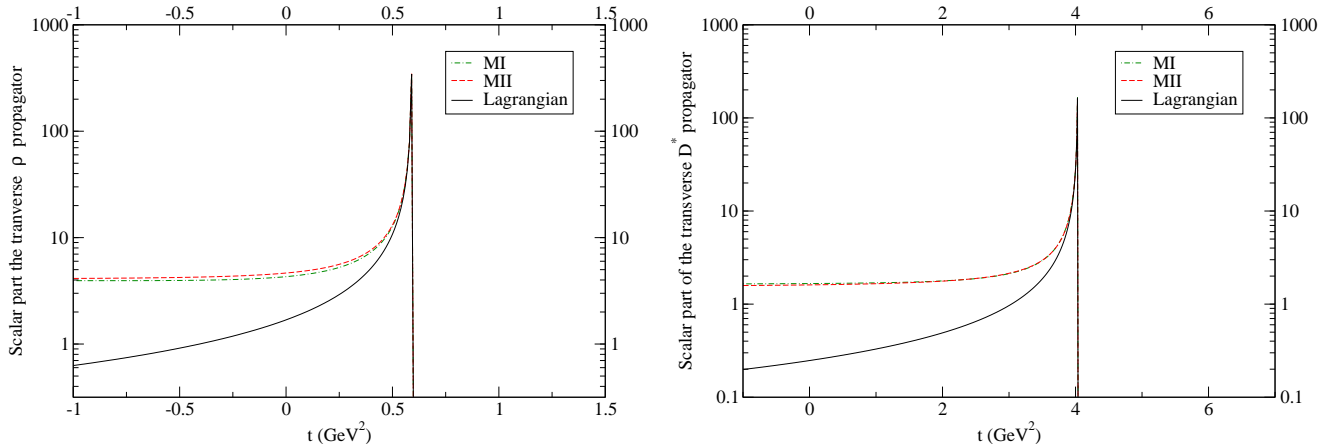


FIG. 4: (Color online) Scalar parts of the transverse ρ and D^* meson propagators near their respective pole.

of $F_{\rho\bar{D}(D)}^0$ is suppressed and the energy dependence of the coefficient proportional to the J/ψ momentum of $F_{J/\psi D(\bar{D})}^0$ is quite different.

Turning to the comparison between MI and MII, we note that the vertices are quite similar both in their overall magnitude and their energy-dependence with the exception of the plotted coefficient of $F_{\pi\bar{D}(D^*)}$. For large space-like separation, large fluctuations appear for MII. This can be linked to the difficulty of carrying out the principal value integral in Eq. (39) due to the large oscillations in the heavy quark form factor in the loop integral. As seen in Fig. 5, increasing the number of numerical evaluations reduces the fluctuations. Although, not apparent in the figure, this problem exists for all vertices with a light meson.

Finally, the four-point coefficients of the form factors $F_{\pi J/\psi\bar{D}D^*}$ and $F_{\rho J/\psi\bar{D}D}$ proportional to the metric tensor are plotted in Fig. 6 for three center-of-mass energies. We note that the form factor used in the Lagrangian approach of Ref. [32] is very suppressed and quite flat compared to the NJL equivalent. Moreover, the differences between the form factors for MI and MII are slightly more pronounced than observed for the three-point functions at least in terms of magnitude.

C. Cross sections

The transition amplitudes can be found in Appendix D. The cross sections are plotted in Figs 7 and 8.^{6,7} We first note that the results for both MI and MII are very similar for small \sqrt{s} and differ only slightly in magnitude for larger values, and therefore the introduction of two additional parameters in MII is probably not justified. Comparison with the results of the phenomenological Lagrangian study of Ref. [32] shows significant differences with MI from

⁶ Because of mixing between open charmed mesons subtle cancellations occur between sub-amplitudes. For the process $\pi + J/\psi \rightarrow (\bar{D} + D^*) + (D + \bar{D}^*)$, for example, this happens between the D^- and D_1^- -exchange channels, and between the D^{*-} and D_0^{*-} -exchange channels. The requirement that they cancel can be traced back to the tensorial decomposition used to split the transverse and longitudinal parts of the vector and axial-vector Dirac structures Eq. (26). This splitting then induces two $1/q^2$ factors where q is the momentum flowing through the propagator. One is absorbed in the transverse projector of the vector particle propagator, while the other is further split between the two vertex functions sandwiching the spin-0 propagator. As $q^2 \rightarrow 0$, divergences appear. Analytically, when all the sub-amplitudes are summed, they cancel; the splitting being artificial. However, these cancellations amount to subtracting large numbers. This leads to a numerical integration problem. Indeed, for certain \sqrt{s} , the quadrature method employed can require evaluations at points close to $q^2 = 0$. To deal with this problem, we force the cancellations within a small radius centered around $q^2 = 0$. In some sense, this is an estimation of the numerical precision associated with the evaluations of the vertices and the propagators. The more precise the evaluations are, the better the cancellation is. A radius value of 0.05 GeV^2 is used here. Relics of the incomplete cancellations usually still remain in the form of small bumps in the data as seen in Fig. 7 around $\sqrt{s} = 4.4 \text{ GeV}$ and $\sqrt{s} = 4.8 \text{ GeV}$ for both $\pi + J/\psi \rightarrow (\bar{D} + D^*) + (D + \bar{D}^*)$ and $\pi + J/\psi \rightarrow \bar{D}^* + D^*$ ($\pi + J/\psi \rightarrow \bar{D} + D$ does not have divergences).

⁷ In order to assess the effect of the finite current mass, the cross section for $\pi + J/\psi \rightarrow \bar{D} + D$ was re-evaluated with a zero current mass. It was found that the deviation is small and no greater than 3.2% at 5 GeV and less than 1.5% near threshold.

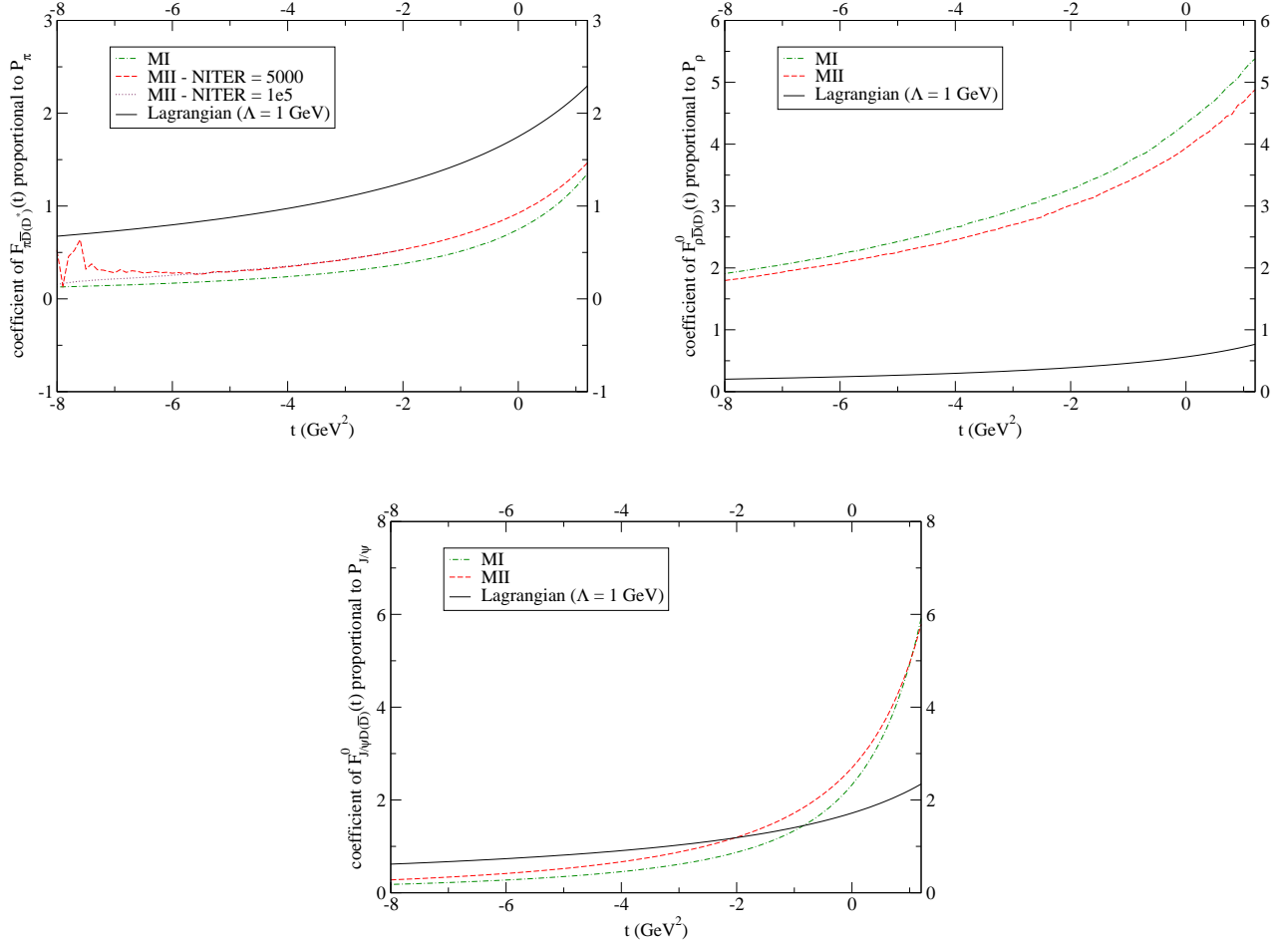


FIG. 5: (Color online) Examples of three-point vertices.

the onset. We note that the maxima of the pion dissociation cross section for $\pi + J/\psi \rightarrow (\bar{D} + D^*) + (D + \bar{D}^*)$ and $\pi + J/\psi \rightarrow \bar{D}^* + D^*$ are smaller by about 50% than those found in the previous non-local NJL study [22] and in the potential model approach [5].⁸ Since in the potential model, the spin-orbit interaction is not modeled the $\pi + J/\psi \rightarrow \bar{D} + D$ process is not evaluated [7], and a comparison can be made only with Ref. [22]. Contrary to the two other pion-induced dissociations the maximum for this process is comparable to that of Ref. [22].

A consequence of the mixing between channels is that, it is impossible to consider normal parity sub-amplitudes on their own in order to assess the effect of chiral symmetry since doing so would entail divergences appearing. However, this does not prevent us from considering the effect of the abnormal sub-amplitude on $\pi + J/\psi \rightarrow (\bar{D} + D^*) + (D + \bar{D}^*)$ process. In Fig. 9, we observe a reduction of the cross section near threshold when the abnormal contribution [\mathcal{M}_{2b} of Appendix D] is removed. Specifically, the maximum ($\sqrt{s} \approx 3.92$ GeV) is seen to decrease by 14%, which is far less than what was found in phenomenological Lagrangian approach of Ref. [32].

For the dissociation by the ρ meson, we estimate a maximal cross section for $\rho + J/\psi \rightarrow (\bar{D} + D^*) + (D + \bar{D}^*)$ comparable to what is found in the potential model [5], while we find a maximum for $\rho + J/\psi \rightarrow \bar{D}^* + D^*$ which is an order of magnitude larger. Finally, the trends of the energy behaviors of all ρ -induced dissociations are similar to those found in Ref. [5].

⁸ In Refs [22] and [5] specific charged channels are plotted, while here we present isospin averaged cross sections. In order to make contact with these studies, the $\pi(\rho) + J/\psi \rightarrow (\bar{D} + D^*) + (D + \bar{D}^*)$ cross section has to be divided by two.

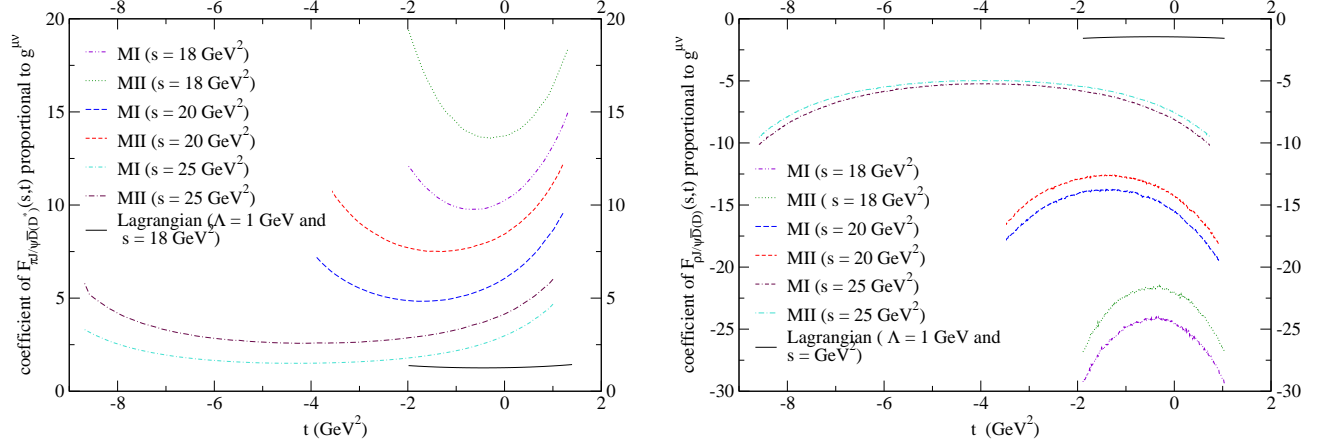


FIG. 6: (Color online) Examples of four-point vertices.

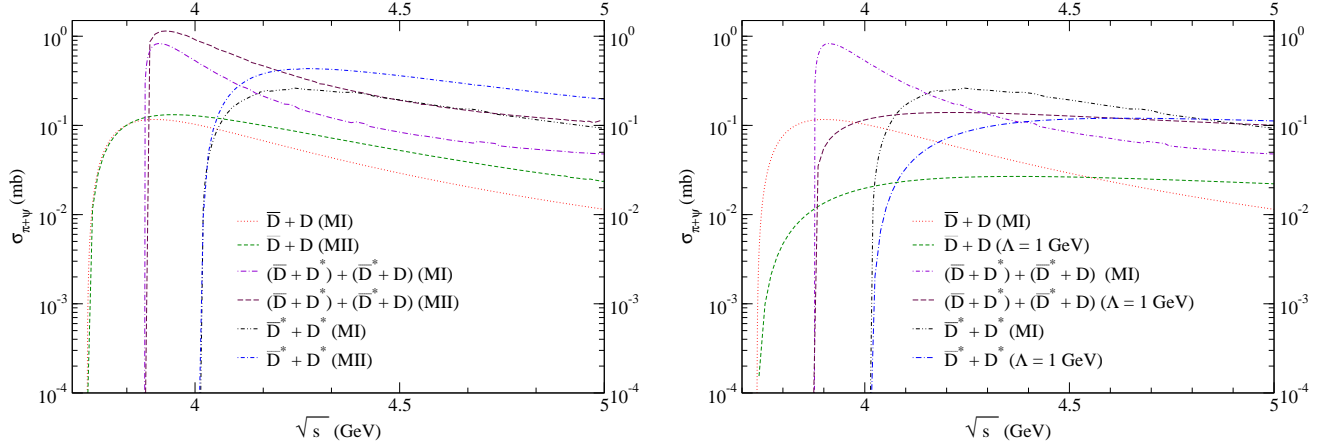


FIG. 7: (Color online) cross sections for the J/ψ -dissociation by a pion. Right panel is a comparison between MI and MII, while the left panel is one between MI and the results from the phenomenological Lagrangian study of Ref. [32] for $\Lambda = 1$ GeV.

VI. CONCLUSION AND OUTLOOK

In Ref. [32], the absolute values of the strength of π - and ρ -induced dissociations depended on the choice of form factors and the techniques used to fix their absolute normalizations, which put into question the robustness of the model. To address this problem, a non-local NJL similar to that of Refs [22, 34] was presented. The vertex form factors were then calculated from the underlying quark structure, thus reducing some of the uncertainties found in the previous study of Ref. [32]. We further utilized the fact that in the non-local version, quark form factors can be chosen in order to confined analytically the light-quark propagator, i.e., the light quark propagator then has no poles. Doing so permitted us to calculate the dissociation cross sections by a ρ meson. However, it was impossible to asset the effect of chiral symmetry since mixing between channels prevented the removal of the sub-amplitudes where chiral partners are exchanged. This problem did not affect the abnormal parity term for $\pi + J/\psi \rightarrow (\bar{D} + D^*) + (D + \bar{D}^*)$. Turning it off then lead to a reduction near threshold as expected. But this decrease was far less substantial than the one observed in the phenomenological Lagrangian approach of Ref. [32].

Further work could include calculating the dissociation of higher charmonia as it is relevant within the context of sequential charmonia melting in the QGP [50]. This would entail improving the heavy-quark four-point interaction

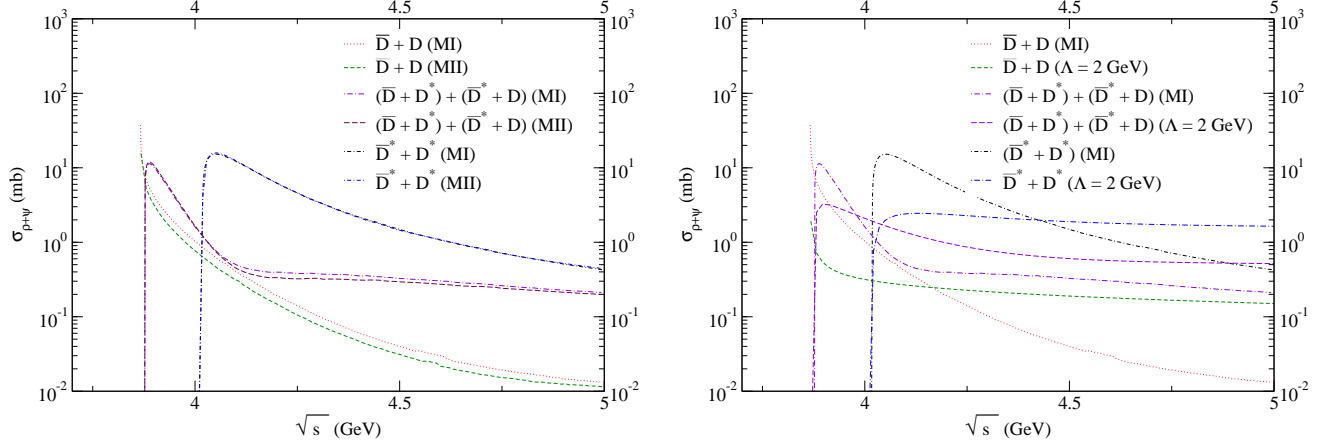


FIG. 8: (Color online) cross sections for the J/ψ -dissociation by a ρ meson. Right panel is a comparison between MI and MII, while the left panel is one between MI and the results from the phenomenological Lagrangian study of Ref. [32] for $\Lambda = 2$ GeV.

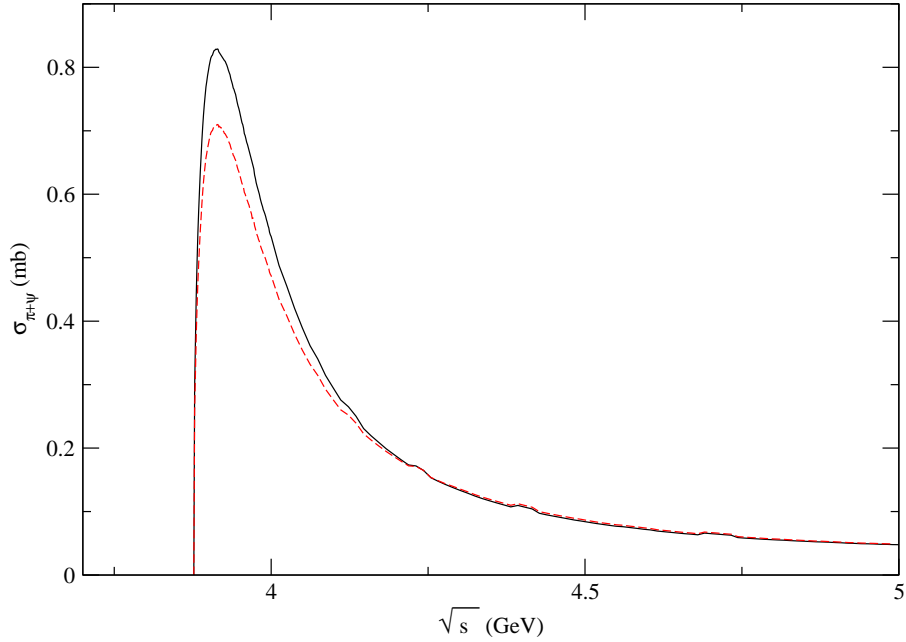


FIG. 9: (Color online) Effect of abnormal parity content on the $\pi + J/\psi \rightarrow (\bar{D} + D^*) + (D^* + D)$ cross section. The dashed and solid lines correspond to cross sections without and with the abnormal parity sub-amplitude.

kernels in such a way that they could sustain higher resonances. Similarly, other light mesons and, potentially, open strange mesons should be considered. Finally, calculating semi-leptonic decay constants and other observables, such as the electromagnetic pion form factor, could lead to an improvement in the modeling, which would then increase the confidence in the overall magnitude of J/ψ -dissociation cross sections.

Acknowledgments

This work was funded in part by the Natural Sciences and Engineering Research Council of Canada, and by the Fonds Nature et Technologies of Quebec.

APPENDIX A: ANALYTIC CONTINUATION

In order to calculate the various loop integrals, an analytic continuation to Euclidean space is needed. In perturbation theory, the usual prescription is the Wick rotation, i.e., for the loop momentum: $k^0 \rightarrow ik_4$, which ensures that the Feynman boundary condition is encoded and that only the relevant poles are picked up [52]. For a model with analytic confinement, a problem arises. This can be made explicit by examining an example.

Consider the loop integral of Eq. (30) for the self-energy of a light meson after a Wick rotation

$$iJ_{ij}(P^2) = -i \int dk_E f_q^2(k_E - \eta\bar{P}) f_q^2((k_E + (1-\eta)\bar{P})) \times \text{Tr} \left[\Gamma_i S_q(k_E - \eta\bar{P}) \tilde{\Gamma}_j S_q((k_E + (1-\eta)\bar{P})) \right] \quad (\text{A1})$$

where an arbitrary momentum shift of the loop momentum parametrised by η has been done and $\bar{P} = (-iP^0, \vec{P})$ with $\bar{P}^2 = -P^2$. Note that the squared light-quark form factor has a square-root dependency since it is defined through Eq. (16) in the Hartree approximation. Furthermore, in Euclidean space, the arguments of the form factors and the quark propagators are in general complex. The conjunction of these two elements can then lead to the appearance of branch cuts making the integrand ill-behaved.

To make this explicit, the chiral limit of the loop integral is taken, namely

$$J(P^2)_{ij} = - \int dk_E \sqrt{\frac{[1 - e^{-\mu z - \eta}][1 - e^{-\mu z_{1-\eta}}] e^{-\mu(z - \eta z_{1-\eta})}}{z_{-\eta} z_{1-\eta}}} g(k_E^2, k_E \cdot \bar{P}, \bar{P}^2) \quad (\text{A2})$$

where the arguments are defined as $z_\delta = (k_E + \delta\bar{P})^2$ and the function $g(k_E^2, k_E \cdot \bar{P}, \bar{P}^2)$ is the product of the Dirac and flavor traces. An Euclidean coordinate transformation is then performed to go from the Cartesian coordinate system to the spherical coordinate one. This is done through [52]

$$k_E = (k_4, \vec{k}) \rightarrow (ky, k\sqrt{1-y^2}\sqrt{1-x^2}\cos\phi, k\sqrt{1-y^2}\sqrt{1-x^2}\sin\phi, k\sqrt{1-y^2}x). \quad (\text{A3})$$

Furthermore, to reduce the number of non-trivial integrals to carry out the fermion-loop is evaluated in the rest-frame of the meson. The complex arguments become

$$z_{-\eta} = k^2 + 2i\eta ky P^0 - \eta^2 P^2, \quad z_{1-\eta} = k^2 - 2i(1-\eta)ky P^0 - (1-\eta)^2 P^2 \quad (\text{A4})$$

with $P = (m_M, 0)$.

For the case of $P^2 = m_\rho^2$, both the real and imaginary parts of the integrand with the trace function g factored out⁹ are plotted as a function of k in Fig. 10 for $y = 0.9$ and two values of η . We note that for $\eta = 0.1$ the imaginary part has several discontinuities which occur when the real part is zero. However, for $\eta = 0.45$, both the real and imaginary parts are smooth functions of k . This latter statement turns out to be true for all y in $[-1, 1]$. Moreover, such a behavior can be identified for a range of η values. It is then possible to evaluate the integral for several η s within this range and check that the results are equal as expected from translational invariance.

We note that by choosing $\eta = \frac{1}{2}$ the arguments of the square-root becomes real and positive for all value of k and y . In other words, the two squared light-quark form factors are complex conjugate of each other. It is important to remark that this is the case only because the evaluation of the fermion-loop is carried in the rest-frame of the meson. Thus by doing the appropriate shift of momentum, the evaluation of the integral in the light-meson's rest-frame is numerically tractable. Moreover, this technique can be applied straight-forwardly to loop integrals of three- and four-point correlations.

⁹ An overall minus sign and the constant numerical factor have also been omitted.

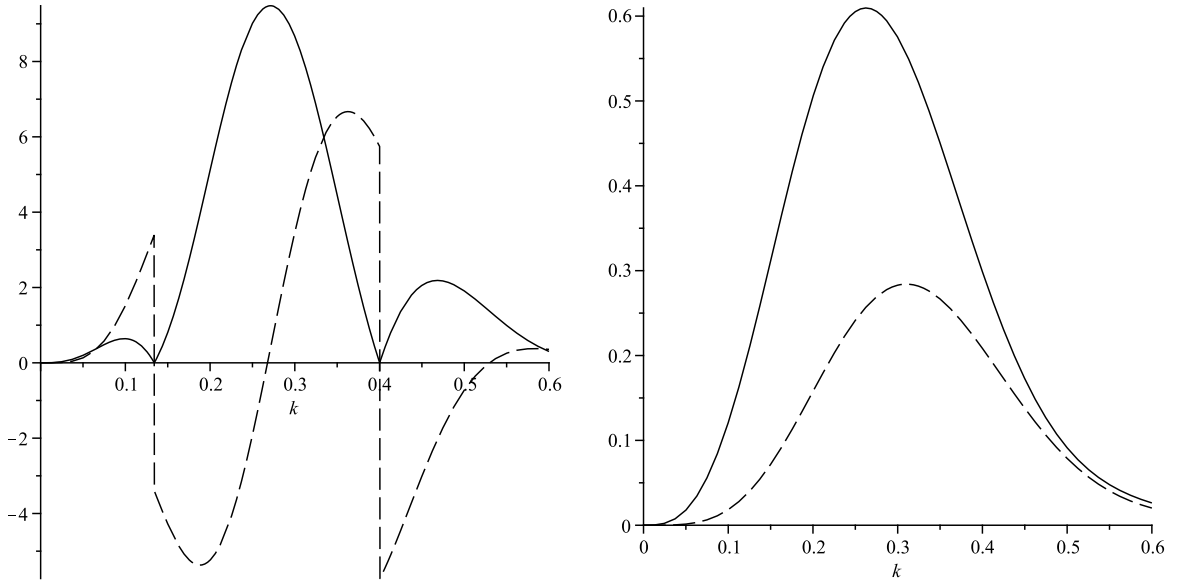


FIG. 10: Real and imaginary parts of the integrand with the trace function omitted. The solid and dash curves are the real and imaginary parts respectively. The left panel is for $\eta = 0.1$ while the right panel is for $\eta = 0.45$.

However, the above procedure cannot be used when evaluating correlation functions with no external light-meson. The simplest example is for the open charmed self-energies where there is only one squared light-quark form factor rather than two. The requirement that there are no branch cuts can then be implemented by shifting the loop momentum in such a way that the integral reads

$$iJ(P^2)_{ij} = -i \int dk_E f_Q^2(k_E + \bar{P}) f_q^2(k_E) \text{Tr} \left[\Gamma_i S_q(k_E) \tilde{\Gamma}_j S_Q((k_E + \bar{P})) \right]. \quad (\text{A5})$$

The argument of the squared light-quark form factor is then always positive and real. However, doing so does leave the possibility that for a certain P^2 the Euclidean heavy quark propagator can go on its mass-shell for some of the k_E -integral points. The required continuation prescription can then be found by going back to the Feynman boundary condition. The heavy quark denominator in the loop integral can be written in Euclidean Cartesian coordinates as

$$(k_E + \bar{P}) + m_Q^2 = k_4^2 + |\vec{k}|^2 - 2ik_4 m_M - m_M^2 + m_Q^2 \quad (\text{A6})$$

where m_M is the meson mass. When $|\vec{k}| = 0$ and $P^2 = 0$, the poles are at $\pm im_Q$ and the Feynman prescription dictates that only the positive pole residue should contribute to the line integral. Keeping the meson mass to zero, but increasing $|\vec{k}|$, we note that the poles move away from the origin. Thus the contour depicted in upper-left panel of Fig. 11 is equivalent to the Wick continuation. Reinstating a meson mass leads to two cases. The first one is when $m_M < m_Q$. For a null loop three-momentum, the poles are on each side of the real k_4 -axis and as $|\vec{k}|$ increases they move away from each other. In this case, there is again no need to alter the contour. The second case, which is more interesting, occurs when $m_H > m_Q$. Both poles are in the upper part of the complex plane for $|\vec{k}| = 0$. One of the pole eventually migrates to the lower half-plane as the loop three-momentum is increased. As this pole crosses the real k_4 -axis a jump occurs in the line integral. This is due to the fact that by evaluating the line integral along the k_4 -axis, the residue of the pole, which in the limit where $m_M = 0$ and $|\vec{k}| = 0$ should not contribute to the integral, is included. The solution is then to deform the contour as in the lower-right panel of Fig. 11 to exclude this pole between $|\vec{k}| = 0$ and $|\vec{k}| = \sqrt{m_M^2 - m_Q^2}$ where the latter point is found under the condition $k_4 = 0$, i.e., when the pole is on the real k_4 -axis and is about to go into the lower half-plane.

The above example is one of two possible scenarios generally encountered. The other one happens when $P \rightarrow -P$ in Eq. (A5). For $m_H > m_Q$ both poles start in the lower half-plane. Thus, the contour has to be deformed now to include the pole required by the Feynman boundary condition for the $|\vec{k}|$ -interval where it is in the lower half-plane.

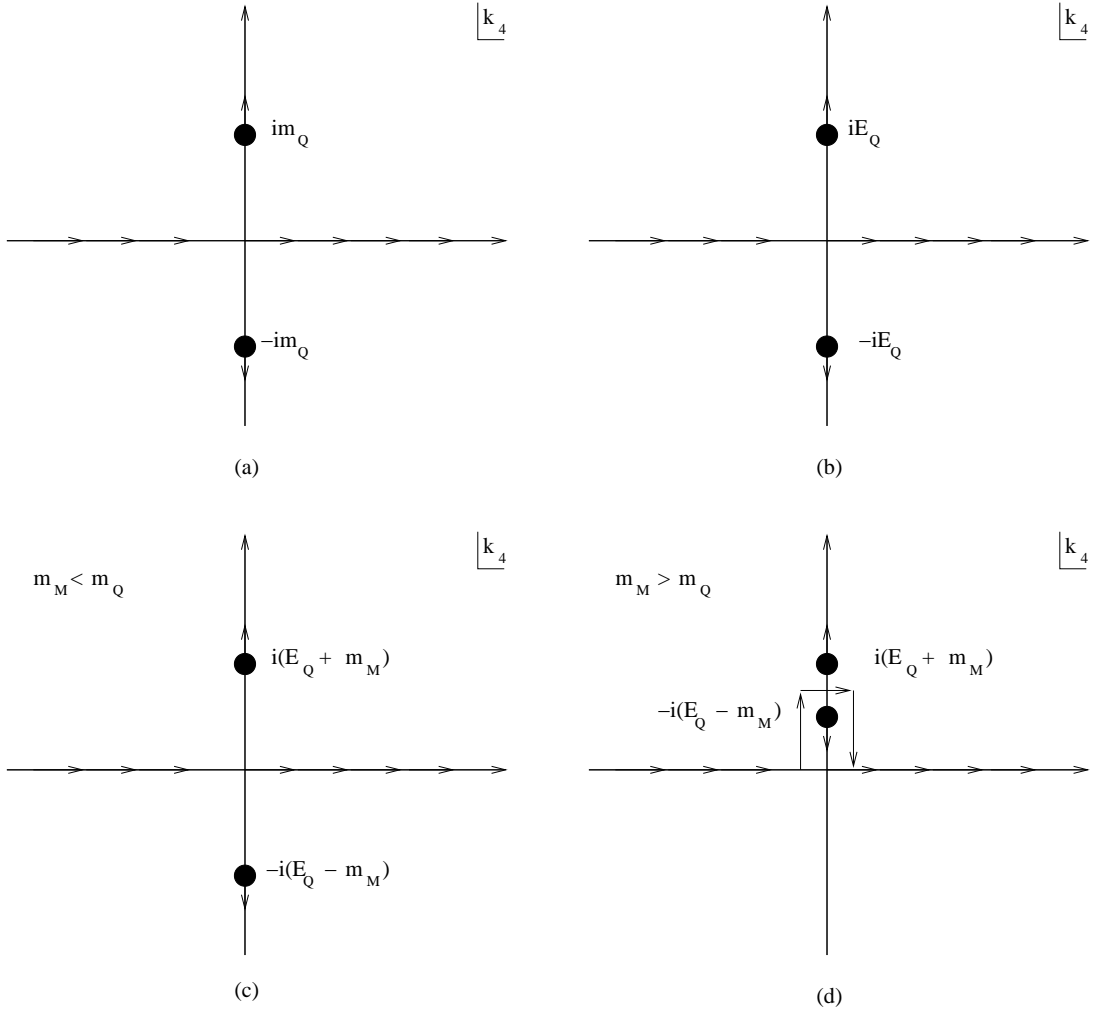


FIG. 11: Line contours for evaluating the open charmed self-energies – (a) $m_H = 0$ and $|\vec{k}| = 0$, (b) $m_H = 0$ and $|\vec{k}| \neq 0$, (c) $m_H < m_Q$ and $|\vec{k}| \neq 0$, and $m_H > m_Q$ and $|\vec{k}| \neq 0$. The arrows on the poles indicate in which direction they moved as $|\vec{k}|$ is increased. The Feynman boundary condition implies that all the contours are closed in the upper-half of the complex plane (not shown here).

This description can be systematically extended to higher-point correlation functions. The final integration prescription in Euclidean space is then, after choosing the appropriate loop momentum flow, to evaluate the principal value of the line integral and add or subtract the appropriate residues.

APPENDIX B: ISOVECTOR AXIAL WARD IDENTITY

It is important to verify that the approximation schemes for the quark and meson propagators are consistent with each other and do not break chiral symmetry in the chiral limit. In our model, the divergences of local currents are not zero. Rather residual terms due to the non-local interactions are left. This problem of constructing a gauge-invariant non-local theory is well studied and we refer the interested reader to the Refs [33, 34, 51] for a complete treatment. In particular, in Ref. [34] the vector current is explicitly constructed and the related Ward identity is checked. Thus, only the isovector axial Ward identity has to be ascertained in order to ensure that chiral symmetry is valid within the approximation context.

For the isovector axial symmetry, its Ward identity is [40]

$$P_\mu \Gamma_5^{a\mu} = \{S^{-1}(p_2) \gamma_5 + \gamma_5 S^{-1}(p_1)\} \frac{\tau^a}{2}. \quad (\text{B1})$$

where the momentum flows are given in Fig. 12.¹⁰ Two cases are considered. The first one is when there are

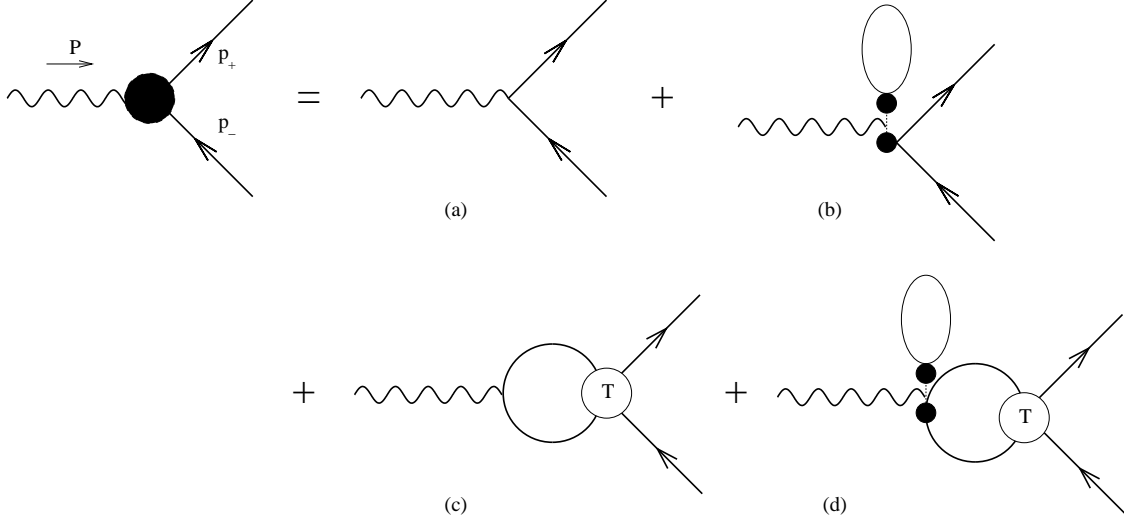


FIG. 12: Contributions to the effective isovector axial vertex. The diagram (a) is the local contribution while diagrams (b), (c), and (d) are the non-local contributions.

only scalar and pseudo-scalar four-quark couplings, while the second one includes mixing due to the introduction of a vector and axial channels. In both cases, the term due to the current quark mass is omitted. For the first case, they are four different contributions to the isovector axial vertex. These are depicted in Fig. 12. The first non-local contribution to the divergence (diagram labeled b in Fig. 12) is due to a scalar fermion-loop which can be inferred from Eq. (13) of Ref. [34]. Summing the local and first non-local terms yields

$$\begin{aligned} P_\mu \tilde{\Gamma}_5^{a\mu} &= P_\mu \gamma^\mu \gamma_5 \frac{\tau^a}{2} + P_\mu J_S^{5a\mu}(P) \\ &= \{S_q^{-1}(p_2) \gamma_5 + \gamma_5 S_q^{-1}(p_1) + i f_q(p_1) f_q(p_2) \gamma_5 I_S(P)\} \frac{\tau^a}{2} \end{aligned} \quad (\text{B2})$$

where the scalar fermion-loop is defined as

$$I_S(P) = G_S \int dk f_q(k) \text{Tr} [S_q(k)] (f_q(k+P) + f_q(k-P)). \quad (\text{B3})$$

Next, the contributions due to the pionic resonance in the absence of mixing [diagrams (c) and (d) of Fig. 12] can be cast as

$$\Gamma_{PS}^{5b} = -i \frac{G_P f_q(p_1) f_q(p_2)}{1 - G_P J_{PP}(P)} \gamma_5 \tau^a \int dk f_q(k_+) f_q(k_-) \text{Tr} \left[\gamma_5 \tau^a S_q(k_+) P_\mu \tilde{\Gamma}_5^{b\mu} S_q(k_-) \right]. \quad (\text{B4})$$

Inserting Eq. (B2) into the above equation yields the final expression for

$$\begin{aligned} \Gamma_{PS}^{5b} &= -i \frac{f_q(p_1) f_q(p_2)}{1 - G_P J_{PP}(P)} \gamma_5 \frac{\tau^b}{2} [1 - G_P J_{PP}(P)] I_S(P) \\ &= -i f_q(p_1) f_q(p_2) \gamma_5 \frac{\tau^b}{2} I_S(P). \end{aligned} \quad (\text{B5})$$

¹⁰ From Eq. (12), it is expected that for a finite current mass: $P_\mu \Gamma_5^{a\mu} = 2m_c^q \cdot \gamma_5 \frac{\tau^a}{2}$.

Summing this contribution and that of Eq. (B2) verifies the axial Ward identity.

Adding the vector and axial channels leads to an additional contribution to Eq. (B2) due to the vector insertion in the fermion-loop. The divergence of the resulting non-local current in momentum-space is inferred from Eq.(10) of Ref. [34] and reads

$$P_\mu J_V^{5a\mu}(P) = if_q(p_1)f_q(p_2)I_V(P)\frac{\not{P}}{\sqrt{P^2}}\gamma_5\frac{\tau^a}{2} \quad (\text{B6})$$

where the vector fermion-loop is

$$I_V(P) = G_V \int dk \text{Tr} \left[\frac{\not{P}}{\sqrt{P^2}} S_q(k) \right] f_q(k) (f_q(k+P) - f_q(k-P)). \quad (\text{B7})$$

The contribution due to the pion intermediate state is then

$$\Gamma_{PS}^{5b} = -if_q(p_1)f_q(p_2) \left\{ I_S(P) + \frac{\not{P}}{\sqrt{P^2}} I_V(P) \right\} \gamma_5 \frac{\tau^b}{2} \quad (\text{B8})$$

which again cancels both the second term of Eq. (B2) and Eq. (B6) thus verifying the axial Ward identity for this extension.

APPENDIX C: DECAYS

1. $g_{\pi D^* D}$ coupling

For the dissociation processes studied, all three-point vertices are evaluated with one external particle off-shell. Moreover, for most of them the kinematics do not allow to have all three mesons on-shell. One exception is for the $D^* \rightarrow D + \pi$ decay process which has been measured experimentally by CLEO [48]

We then wish to use this experimental information to constrain the parameter set. To do so, the expression of the decay width as a function of the on-shell three-point coupling is written down:

$$\Gamma_{D^* \rightarrow D^+ + \pi^0} = \frac{g_{\pi D^* D}^2 |\vec{P}_\pi|^3}{48m_{D^*}^2} \quad (\text{C1})$$

where $|\vec{P}_\pi|$ is the centre-of-mass three-momentum. The second step then consists in relating the coupling to the the extended NJL model. The associated meson form factor can be decomposed into

$$F_{D^* \rightarrow D^+ + \pi^0}^\mu = F_0 P_\pi^\mu + F_1 P_{D^*}^\mu, \quad (\text{C2})$$

with the coupling given by

$$g_{\pi D^* D} = \sqrt{2}(F_0 - F_1) \quad (\text{C3})$$

where four-momentum conservation $P_{D^*} = P_\pi + P_D$ and orthogonality $\epsilon(P_{D^*}) \cdot P_{D^*} = 0$ have been used, and the factor $\sqrt{2}$ is to account for isospin (the coupling $g_{\pi D^* D}$ being defined to be equal to $g_{D^* \rightarrow D^0 + \pi^+}$ [48]).

2. J/ψ decay into a dilepton

We now turn to the calculation of the decay of the J/ψ into a dilepton. Fig. 13 shows the contributions to the effective quark-photon vertex. It is assumed that the dominant behavior will be given by diagrams at leading order in $1/N_C$. Thus, only the transition due to constituent quark loop in the direct channel will be considered; exchange diagrams and mesonic fluctuations are ignored. It is important to note that this approximation is consistent with the Ward identity [34]. The transition amplitude of an on-shell J/ψ into a photon is then

$$\begin{aligned} i\mathcal{M}_{\psi\gamma}^{\mu\nu}(P) &= - \int dk \text{Tr} [i\chi^\mu(k, P) iS_Q(k_-) i\Gamma_{EM}^\nu(k, P) iS_Q(k_+)] \\ &= -g_\psi e Q T_\alpha^\mu \int dk f_Q(k_+) f_Q(k_-) \text{Tr} [\gamma^\alpha S_Q(k_-) \Gamma_{EM}^\nu(k, P) S_Q(k_+)] \\ &= -g_\psi e Q T^{\mu\nu} [I_T^L(P) + I_T^{NL}(P)] \end{aligned} \quad (\text{C4})$$

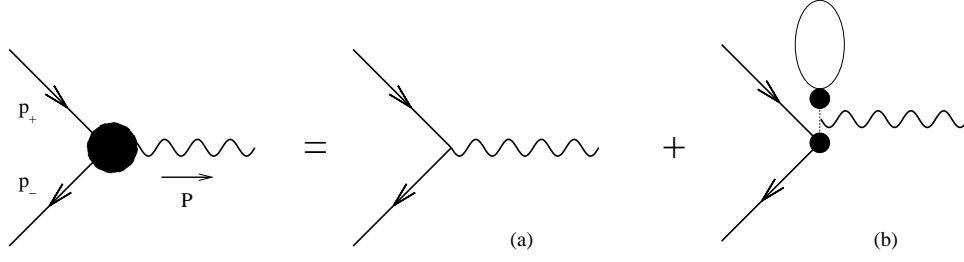


FIG. 13: Contributions to the effective quark-photon vertex for the decay of the J/ψ into a dilepton. Diagram (a) and (b) are the local and non-local contributions respectively. The latter is due to a fermion-loop with a vector insertion.

where Q is the electric charge of the heavy quark, $e = |e|$, the minus sign in front of the integral is due to the fermion-loop, and the wavefunction meson label is suppressed. The coupling constant between the full current and the photon field, A , is derived from

$$\mathcal{L}_{EM} = -eQJ_{EM}^\mu(x)A_\mu(x). \quad (C5)$$

And coupling the photon to a dilepton finally yields the decay width

$$\Gamma_{\psi \rightarrow l^+ l^-} = \frac{e^2}{6\pi} \left[\frac{\mathcal{M}_{\psi\gamma}^2}{m_\psi^4} \right] \frac{|\vec{P}|^3}{m_\psi^2} \quad (C6)$$

where $|\vec{P}|^2 = \frac{m_\psi^2}{4} - m_l^2$.

The main ingredient left to specify is thus the effective electromagnetic vertex. In the heavy quark sector, only a vector coupling is introduced. Thus there is only one correction term to the local vertex and we can write

$$\Gamma_{EM}^\mu(p, P) = \gamma^\mu + \Gamma_V^\mu(p, P) \quad (C7)$$

where

$$\Gamma_V^\mu(p, P) = f_Q(p_+)f_Q(p_-)\gamma^\nu [iG_V I_\nu^\mu(P)] \quad (C8)$$

and

$$I_\nu^\mu(P) = - \int_0^1 d\lambda \int dk \text{Tr} [\gamma_\nu S_Q(k)] \frac{\partial}{\partial k^\mu} f_Q(k + \lambda P) f_Q(k - (1 - \lambda)P). \quad (C9)$$

Inserting the electromagnetic vertex into the transition amplitude gives

$$\begin{aligned} i\mathcal{M}_{\psi\gamma}^{L;\mu\nu}(P) &= -g_\psi e Q T_\alpha^\mu \int dk f_Q(k_+) f_Q(k_-) \text{Tr} [\gamma^\alpha S_Q(k_-) \gamma^\nu S_Q(k_+)] \\ &= -g_\psi e Q T^{\mu\nu} I_T^L \end{aligned} \quad (C10)$$

and

$$i\mathcal{M}_{\psi\gamma}^{NL;\mu\nu}(P) = -g_\psi e Q T^{\mu\beta} [G_V J_\psi^T(P^2)] I_\beta^\nu(P) = -g_\psi e Q T^{\mu\nu} I_T^{NL} \quad (C11)$$

where, for the non-local term, Eqs. (30) and (31) have been used and the scalar integrals are defined as

$$I_T^L = 4N_C \int dk f_Q(k_+) f_Q(k_-) \frac{\left(m_Q^2 + \frac{P^2}{4} - \frac{k^2}{3} - \frac{2}{3} \frac{(k \cdot P)^2}{P^2} \right)}{\left[k_+^2 - m_Q^2 \right] \left[k_-^2 - m_Q^2 \right]} \quad (C12)$$

and

$$I_T^{NL} = \frac{8N_C}{3} \int_0^1 d\lambda \int dk \frac{\left(k^2 - \frac{(k \cdot P)^2}{P^2} \right)}{k^2 - m_Q^2} \frac{d}{dk^2} f_Q(k + \lambda P) f_Q(k - (1 - \lambda)P). \quad (C13)$$

From the non-local scalar integrals, we note that the final result will dependent on the interpolation path. This is due to the fact that the coupling between the photon and the J/ψ is transverse and, thus, not constrained by the underlying current conservation.

3. Pion decay constant

The leptonic decay of the pion into a muon and a muonic anti-neutrino can be studied by considering the coupling of the pion-field to the isovector axial current [53]. Formally, the coupling is inferred from the matrix element

$$\int dx e^{iP \cdot x} \langle 0 | T \left(\pi^a(x) J_5^{b\mu}(0) \right) | 0 \rangle \quad (\text{C14})$$

where translational invariance has been invoked and the pion momentum is outgoing. Near the pion pole, it becomes [52]

$$\int dx e^{iP \cdot x} \langle 0 | T(\pi^a(x) J_5^{b\mu}(0) | 0) \rightarrow \frac{i\mathcal{M}_{AP}^\mu \delta^{ab}}{P^2 - m_\pi^2} \quad (\text{C15})$$

where the transition amplitude \mathcal{M}_{AP}^μ is given by

$$i\mathcal{M}_{AP}^\mu P_\mu \chi^a(p, P) = [i\Gamma_{PS}^{5a}(P^2 - m_\pi^2)]|_{P^2 \approx m_\pi^2}. \quad (\text{C16})$$

The latter is a consequence of the isovector axial current being dominated by the pion-resonance contribution near the pole [40]. Moreover, for leptonic decay, the transition amplitude is usually parametrised as

$$i\mathcal{M}_{AP}^\mu = if_\pi P^\mu. \quad (\text{C17})$$

Putting everything together leads to the expression

$$[i\Gamma_{PS}^{5a}(P^2 - m_\pi^2)]|_{P^2 \approx m_\pi^2} = if_\pi m_\pi^2 \chi^a(p, P). \quad (\text{C18})$$

The evaluation of the pion decay constant is thus reduced to that of the pseudo-scalar contribution near the pion pole. Consider first a theory without any vector or axial four-quark couplings. The pseudo-scalar contribution near the pion pole is given at leading N_C order by

$$\begin{aligned} \Gamma_{PS}^{5b} \approx & \frac{\chi^a(p, P)}{P^2 - m_\pi^2} \frac{g_\pi}{2} \left\{ (1 - G_P J_{PP}(P)) \delta^{ab} I_S(P) \right. \\ & \left. + 2m_c^q \int dk f_q(k_+) f(k_-) \text{Tr} [\gamma_5 \tau^a S_q(k_+) \gamma_5 \tau^b S_q(k_-)] \right\} \end{aligned} \quad (\text{C19})$$

where the second term is due to finite current quark mass. Using the definition of the pion wavefunction, the pion decay constant is extracted from Eq. (C18) and reads

$$\begin{aligned} f_\pi m_\pi^2 \delta^{ab} = & -m_c^q \int dk \text{Tr} [\bar{\chi}^a(k, P) S_q(k_+) i\gamma_5 \tau^b S_q(k_-)] \\ & + \frac{g_\pi}{2} (1 - G_P J_{PP}(P)) \delta^{ab} I_S(P). \end{aligned} \quad (\text{C20})$$

where at the pole the second term is zero. Note also, that because the quark-pion coupling scales like $1/\sqrt{N_c}$, the pion decay constant will have a $\sqrt{N_c}$ dependence.

Introducing vector and axial couplings, the expression for the pion decay constant then becomes

$$\begin{aligned} f_\pi m_\pi^2 \delta^{ab} = & -m_c^q \int dk \text{Tr} [\bar{\chi}^a(k, P) S_q(k_+) i\gamma_5 \tau^b S_q(k_-)] \\ & + \frac{g_\pi}{2} \Delta_\pi(P) \left\{ I_S(P) + \frac{P}{\sqrt{P^2}} I_V(P) \right\} \delta^{ab}. \end{aligned} \quad (\text{C21})$$

Again, only the first term survives at $P^2 = m_\pi^2$.

Contrary to the electromagnetic decay of the J/ψ into a dilepton, the pion decay constant does not depend on the path. This is due to the fact that the pion couples to the divergence of the isovector axial current, i.e., its longitudinal part, which is entirely determined by the axial Ward identity.

APPENDIX D: SCATTERING AMPLITUDES FOR THE NON-LOCAL NJL MODEL

1. $J/\psi + \pi \rightarrow \bar{D} + D$

$$\mathcal{M}_{1a}^\rho = -F_{\pi D(\bar{D}^*)}^\alpha(t) \mathcal{D}_{\alpha\beta}^{D^*}(p_\pi - p_D) F_{\psi \bar{D}(D^*)}^{\beta\rho}(t), \quad (\text{D1})$$

$$\mathcal{M}_{1b}^\rho = -F_{\pi \bar{D}(D^*)}^\alpha(u) \mathcal{D}_{\alpha\beta}^{D^*}(p_\pi - p_{\bar{D}}) F_{\psi D(\bar{D}^*)}^{\beta\rho}(u), \quad (\text{D2})$$

$$\mathcal{M}_{1c}^\rho = F_{\pi\psi \bar{D}D}^\rho(s, t) \quad (\text{D3})$$

where $t = (p_\pi - p_D)^2$ and $u = (p_\pi - p_{\bar{D}})^2$.

2. $J/\psi + \pi \rightarrow \bar{D} + D^*$

$$\mathcal{M}_{2a}^{\mu\rho} = \sum_i F_{\pi D^*(\bar{D})}^{\mu;i}(t) \mathcal{D}_{ij}^D(p_\pi - p_{D^*}) F_{\psi \bar{D}(D)}^{\rho;j}(t), \quad (\text{D4})$$

$$\mathcal{M}_{2b}^{\mu\rho} = F_{\pi D^*(\bar{D}^*)}^{\mu\alpha}(t) \mathcal{D}_{\alpha\beta}^{D^*}(p_\pi - p_{D^*}) F_{\psi \bar{D}(D^*)}^{\beta\rho}(t), \quad (\text{D5})$$

$$\mathcal{M}_{2c}^{\mu\rho} = F_{\pi \bar{D}(D^*)}^\alpha(u) \mathcal{D}_{\alpha\beta}^{D^*}(p_\pi - p_{\bar{D}}) F_{\psi D^*(\bar{D}^*)}^{\beta\mu\rho}(u), \quad (\text{D6})$$

$$\mathcal{M}_{2d}^{\mu\rho} = F_{\pi\psi \bar{D}D^*}^{\mu\rho}(s, t), \quad (\text{D7})$$

$$\mathcal{M}_{2e}^{\mu\rho} = F_{\pi D^*(\bar{D}_1)}^{\mu\alpha}(t) \mathcal{D}_{\alpha\beta}^{D_1}(p_\pi - p_{D^*}) F_{\psi \bar{D}(D_1)}^{\beta\rho}(t), \quad (\text{D8})$$

$$\mathcal{M}_{2f}^{\mu\rho} = \sum_i F_{\pi \bar{D}(D_0^*)}^{\mu;i}(u) \mathcal{D}_{ij}^{D_0^*}(p_\pi - p_{\bar{D}}) F_{\psi D^*(\bar{D}_0^*)}^{\rho\mu;j}(u) \quad (\text{D9})$$

where $t = (p_\pi - p_{D^*})^2$ and $u = (p_\pi - p_{\bar{D}})^2$.

3. $J/\psi + \pi \rightarrow \bar{D}^* + D^*$

$$\mathcal{M}_{3a}^{\mu\nu\rho} = \sum_i F_{\pi D^*(\bar{D})}^{\nu;i}(t) \mathcal{D}_{ij}^D(p_\pi - p_{D^*}) F_{\psi \bar{D}^*(D)}^{\mu\rho;j}(t), \quad (\text{D10})$$

$$\mathcal{M}_{3b}^{\mu\nu\rho} = \sum_i F_{\pi \bar{D}^*(D)}^{\mu;i}(u) \mathcal{D}_{ij}^D(p_\pi - p_{\bar{D}^*}) F_{\psi D^*(\bar{D})}^{\nu\rho;j}(u), \quad (\text{D11})$$

$$\mathcal{M}_{3c}^{\mu\nu\rho} = F_{\pi D^*(\bar{D}^*)}^{\alpha\nu}(t) \mathcal{D}_{\alpha\beta}^{D^*}(p_\pi - p_{D^*}) F_{\psi \bar{D}^*(D^*)}^{\mu\beta\rho}(t), \quad (\text{D12})$$

$$\mathcal{M}_{3d}^{\mu\nu\rho} = F_{\pi \bar{D}^*(D^*)}^{\mu\alpha}(u) \mathcal{D}_{\alpha\beta}^{D^*}(p_\pi - p_{\bar{D}^*}) F_{\psi D^*(\bar{D}^*)}^{\beta\nu\rho}(u), \quad (\text{D13})$$

$$\mathcal{M}_{3e}^{\mu\nu\rho} = F_{\pi\psi \bar{D}^*D^*}^{\mu\nu\rho}(s, t), \quad (\text{D14})$$

$$\mathcal{M}_{3f}^{\mu\nu\rho} = F_{\pi D^*(\bar{D}_1)}^{\alpha\nu}(t) \mathcal{D}_{\alpha\beta}^{D_1}(p_\pi - p_{D^*}) F_{\psi \bar{D}^*(D_1)}^{\mu\beta\rho}(t), \quad (\text{D15})$$

$$\mathcal{M}_{3g}^{\mu\nu\rho} = F_{\pi \bar{D}^*(D_1)}^{\mu\alpha}(u) \mathcal{D}_{\alpha\beta}^{D_1}(p_\pi - p_{\bar{D}^*}) F_{\psi D^*(\bar{D}_1)}^{\beta\nu\rho}(u) \quad (\text{D16})$$

where $t = (p_\pi - p_{D^*})^2$ and $u = (p_\pi - p_{\bar{D}^*})^2$.

4. $J/\psi + \rho \rightarrow \bar{D} + D$

$$\mathcal{M}_{4a}^{\delta\rho} = \sum_i F_{\rho D(\bar{D})}^{\delta;i}(t) \mathcal{D}_{ij}^D(p_\rho - p_D) F_{\psi \bar{D}(D)}^{\rho;j}(t), \quad (\text{D17})$$

$$\mathcal{M}_{4b}^{\delta\rho} = \sum_i F_{\rho \bar{D}(D)}^{\delta;i}(u) \mathcal{D}_{ij}^D(p_\rho - p_{\bar{D}}) F_{\psi(\bar{D})D}^{\rho;j}(u), \quad (\text{D18})$$

$$\mathcal{M}_{4c}^{\delta\rho} = F_{\rho D(\bar{D}^*)}^{\alpha\delta}(t) \mathcal{D}_{\alpha\beta}^{D^*}(p_\rho - p_D) F_{\psi \bar{D}(D^*)}^{\beta\rho}(t), \quad (\text{D19})$$

$$\mathcal{M}_{4d}^{\delta\rho} = F_{\rho \bar{D}(D^*)}^{\alpha\delta}(u) \mathcal{D}_{\alpha\beta}^{D^*}(p_\rho - p_{\bar{D}}) F_{\psi D(\bar{D}^*)}^{\beta\rho}(u), \quad (\text{D20})$$

$$\mathcal{M}_{4e}^{\delta\rho} = F_{\rho\psi\bar{D}D}^{\delta\rho}(s, t), \quad (\text{D21})$$

$$\mathcal{M}_{4f}^{\delta\rho} = F_{\rho D(\bar{D}_1)}^{\alpha\delta}(t) \mathcal{D}_{\alpha\beta}^{D_1}(p_\rho - p_D) F_{\psi \bar{D}(D_1)}^{\beta\rho}(t), \quad (\text{D22})$$

$$\mathcal{M}_{4g}^{\delta\rho} = F_{\rho \bar{D}(D_1)}^{\alpha\delta}(u) \mathcal{D}_{\alpha\beta}^{D_1}(p_\rho - p_{\bar{D}}) F_{\psi D(\bar{D}_1)}^{\beta\rho}(u) \quad (\text{D23})$$

where $t = (p_\rho - p_D)^2$ and $u = (p_\rho - p_{\bar{D}})^2$.

5. $J/\psi + \rho \rightarrow \bar{D} + D^*$

$$\mathcal{M}_{5a}^{\mu\delta\rho} = \sum_i F_{\rho D^*(\bar{D})}^{\mu\delta;i}(t) \mathcal{D}_{ij}^D(p_\rho - p_{D^*}) F_{\psi \bar{D}(D)}^{\rho;j}(t), \quad (\text{D24})$$

$$\mathcal{M}_{5b}^{\mu\delta\rho} = \sum_i F_{\rho \bar{D}(D)}^{\delta;i}(u) \mathcal{D}_{ij}^D(p_\rho - p_{\bar{D}}) F_{\psi D^*(\bar{D})}^{\mu\rho;j}(u), \quad (\text{D25})$$

$$\mathcal{M}_{5c}^{\mu\delta\rho} = F_{\rho D^*(\bar{D}^*)}^{\mu\alpha\delta}(t) \mathcal{D}_{\alpha\beta}^{D^*}(p_\rho - p_{D^*}) F_{\psi \bar{D}(D^*)}^{\beta\rho}(t), \quad (\text{D26})$$

$$\mathcal{M}_{5d}^{\mu\delta\rho} = F_{\rho \bar{D}(D^*)}^{\alpha\delta}(u) \mathcal{D}_{\alpha\beta}^{D^*}(p_\rho - p_{\bar{D}}) F_{\psi D^*(\bar{D}^*)}^{\mu\beta\rho}(u), \quad (\text{D27})$$

$$\mathcal{M}_{5e}^{\mu\delta\rho} = F_{\rho\psi\bar{D}D^*}^{\mu\delta\rho}(s, t), \quad (\text{D28})$$

$$\mathcal{M}_{5f}^{\mu\delta\rho} = F_{\rho D^*(\bar{D}_1)}^{\mu\alpha\delta}(t) \mathcal{D}_{\alpha\beta}^{D_1}(p_\rho - p_{D^*}) F_{\psi \bar{D}(D_1)}^{\beta\rho}(t), \quad (\text{D29})$$

$$\mathcal{M}_{5g}^{\mu\delta\rho} = F_{\rho \bar{D}(\bar{D}_1)}^{\alpha\delta}(u) \mathcal{D}_{\alpha\beta}^{D_1}(p_\rho - p_{\bar{D}}) F_{\psi D^*(\bar{D}_1)}^{\mu\beta\rho}(u) \quad (\text{D30})$$

where $t = (p_\rho - p_{D^*})^2$ and $u = (p_\rho - p_{\bar{D}})^2$.

6. $J/\psi + \rho \rightarrow \bar{D}^* + D^*$

$$\mathcal{M}_{6a}^{\mu\nu\delta\rho} = \sum_i F_{\rho D^*(\bar{D})}^{\mu\delta;i}(t) \mathcal{D}_{ij}^D(p_\rho - p_{D^*}) F_{\psi \bar{D}^*(D)}^{\nu\rho;j}(t), \quad (\text{D31})$$

$$\mathcal{M}_{6b}^{\mu\nu\delta\rho} = \sum_i F_{\rho \bar{D}^*(D)}^{\nu\delta;i}(u) \mathcal{D}_{ij}^D(p_\rho - p_{\bar{D}^*}) F_{\psi \bar{D}^*(\bar{D})}^{\mu\rho;j}(u), \quad (\text{D32})$$

$$\mathcal{M}_{6c}^{\mu\nu\delta\rho} = F_{\rho D^*(\bar{D}^*)}^{\mu\alpha\delta}(t) \mathcal{D}_{\alpha\beta}^{D^*}(p_\rho - p_{D^*}) F_{\psi \bar{D}^*(D^*)}^{\beta\nu\rho}(t), \quad (\text{D33})$$

$$\mathcal{M}_{6d}^{\mu\nu\delta\rho} = F_{\rho \bar{D}^*(D^*)}^{\alpha\nu\delta}(u) \mathcal{D}_{\alpha\beta}^{D^*}(p_\rho - p_{\bar{D}^*}) F_{\psi \bar{D}^*(\bar{D}^*)}^{\mu\beta\rho}(u), \quad (\text{D34})$$

$$\mathcal{M}_{6e}^{\mu\nu\delta\rho} = F_{\rho\psi\bar{D}^*D^*}^{\mu\nu\delta\rho}(s, t), \quad (\text{D35})$$

$$\mathcal{M}_{6f}^{\mu\nu\delta\rho} = F_{\rho D^*(\bar{D}_1)}^{\mu\alpha\delta}(t) \mathcal{D}_{\alpha\beta}^{D_1}(p_\rho - p_{D^*}) F_{\psi \bar{D}^*(D_1)}^{\beta\nu\rho}(t), \quad (\text{D36})$$

$$\mathcal{M}_{6g}^{\mu\nu\delta\rho} = F_{\rho \bar{D}^*(D_1)}^{\alpha\nu\delta}(u) \mathcal{D}_{\alpha\beta}^{D_1}(p_\rho - p_{\bar{D}^*}) F_{\psi \bar{D}^*(\bar{D}_1)}^{\mu\beta\rho}(u), \quad (\text{D37})$$

$$\mathcal{M}_{6h}^{\mu\nu\delta\rho} = \sum_i F_{\rho D^*(\bar{D}_0^*)}^{\mu\delta;i}(t) \mathcal{D}_{ij}^{D_0^*}(p_\rho - p_{D^*}) F_{\psi \bar{D}^*(D_0^*)}^{\nu\rho;j}(t), \quad (\text{D38})$$

$$\mathcal{M}_{6i}^{\mu\nu\delta\rho} = \sum_i F_{\rho \bar{D}^*(D_0^*)}^{\nu\delta;i}(u) \mathcal{D}_{ij}^{D_0^*}(p_\rho - p_{\bar{D}^*}) F_{\psi \bar{D}^*(\bar{D}_0^*)}^{\mu\rho;j}(u) \quad (\text{D39})$$

where $t = (p_\rho - p_{D^*})^2$ and $u = (p_\rho - p_{\bar{D}^*})^2$.

-
- [1] P. Petreczky (2005), hep-lat/0506012.
[2] H. Satz, J. Phys. G **32**, R25 (2006).
[3] T. Matsui and H. Satz, Phys. Lett. B **178**, 416 (1986).
[4] D. Kharzeev, C. Lourenco, M. Nardi and H. Satz, Z. Phys. C **74**, 307 (1997).
[5] T. Barnes, E. S. Swanson, C. Y. Wong and X. M. Xu, Phys. Rev. C **68**, 014903 (2003).
[6] K. Martins, D. Blaschke and E. Quack, Phys. Rev. C **51**, 2723 (1995).
[7] C. Y. Wong, E. S. Swanson and T. Barnes, Phys. Rev. C **62**, 045201 (2000).
[8] C. Y. Wong, E. S. Swanson and T. Barnes, Phys. Rev. C **65**, 014903 (2001).
[9] F. O. Duraes, H. C. Kim, S. H. Lee, F. S. Navarra and M. Nielsen, Phys. Rev. C **68**, 035208 (2003).
[10] F. S. Navarra, M. Nielsen, M. E. Bracco, M. Chiapparini and C. L. S., Phys. Lett. B **489**, 319 (2000).
[11] M. E. Bracco, M. Chiapparini, A. Lozea, F. S. Navarra and M. Nielsen, Phys. Lett. B **521**, 1 (2001).
[12] F. S. Navarra, M. Nielsen, R. S. Marques de Carvalho and G. Krein, Phys. Lett. B **529**, 87 (2002).
[13] F. S. Navarra, M. Nielsen and M. E. Bracco, Phys. Rev. D **65**, 037502 (2002).
[14] R. D. Matheus, F. S. Navarra, M. Nielsen and R. Rodrigues da Silva, Phys. Lett. B **541**, 265 (2002).
[15] F. O. Duraes, S. H. Lee, F. S. Navarra and M. Nielsen, Phys. Lett. B **564**, 97 (2003).
[16] R. S. Azevedo and M. Nielsen, Phys. Rev. C **69**, 035201 (2004).
[17] L. Maiani, F. Piccinini, A. D. Polosa and V. Riquer, Nucl. Phys. A **748**, 209 (2005).
[18] A. D. Polosa, Riv. Nuovo Cimento **23N11**, 1 (2000).
[19] D. Blaschke, G. Burau, Yu. L. Kalinovsky, P. Maris and P. C. Tandy, Int. J. Mod. Phys. A **16**, 2267 (2001).
[20] A. Deandrea, G. Nardulli and A. D. Polosa, Phys. Rev. D **68**, 034002 (2003).
[21] L. Maiani, F. Piccinini, A. D. Polosa and V. Riquer, Nucl. Phys. A **741**, 273 (2004).
[22] M. A. Ivanov, J. G. Korner and P. Santorelli, Phys. Rev. D **70**, 014005 (2004).
[23] V. Laporta, A. D. Polosa, F. Piccinini and V. Riquer, Eur. Phys. J. C **48**, 545 (2006).
[24] S. G. Matinyan and B. Muller, Phys. Rev. C **58**, 2994 (1998).
[25] Z. Lin, C.M. Ko, and B. Zhang, Phys. Rev. C **61**, 024904 (2000).
[26] Z. Lin and C. M. Ko, Phys. Rev. C **62**, 034903 (2000).
[27] K. L. Haglin, Phys. Rev. C **61**, 031902(R) (2000).
[28] K. L. Haglin and C. Gale, Phys. Rev. C **63**, 065201 (2001).
[29] Y. Oh, T. Song, and S.H. Lee, Phys. Rev. C **63**, 034901 (2001).
[30] F. S. Navarra, M. Nielsen, and M. R. Robilotta, Phys. Rev. C **64**, 021901(R) (2001).
[31] A. Bourque, C. Gale, and K. L. Haglin, Phys. Rev. C **70**, 055203 (2004).
[32] A. Bourque and C. Gale, Phys. Rev. C **78**, 035206 (2008).
[33] R. D. Bowler and M. C. Birse, Nucl. Phys. A **582**, 655 (1995).
[34] R. S. Plant and M. C. Birse, Nucl. Phys. A **628**, 607 (1998).

- [35] R. S. Plant and M. C. Birse, Nucl. Phys. A **703**, 717 (2002).
- [36] Y. Nambu and G. Jona-Lasinio, Phys. Rev. **122**, 345 (1961).
- [37] U. Vogl and W. Weise, Prog. Part. Nucl. Phys. **27**, 195 (1991).
- [38] S. Noguera, Int. J. Mod. Phys. E **16**, 97 (2007).
- [39] V. Dmitrašinović, H.-J. Schulze, R. Tegen, and R.H. Lemmer, Annals of Physics **238**, 332 (1995).
- [40] C. D. Roberts and A. G. Williams, Prog. Part. Nucl. Phys **33**, 477 (1994).
- [41] M. Oertel (2000), hep-ph/0012224.
- [42] A. E. Radzhabov and M. K. Volkov, Eur. Phys. J. A **19**, 139 (2004).
- [43] M. Buballa and S. Krewald, Phys. Lett. B **19**, 294 (1992).
- [44] E. E. Salpeter and H. A. Bethe, Phys. Rev. **84**, 1232 (1951).
- [45] R. Alkofer and L. von Smekal, Phys. Rept. **353**, 281 (2001).
- [46] S. Klimt, M. Lutz, U. Vogl and W. Weise, Nucl. Phys. A **516**, 429 (1990).
- [47] R. E. Cutkosky, P. V. Landshoff, D. I. Olive and J. C. Polkinghorne, Nucl. Phys. B **12**, 281 (1969).
- [48] A. Anastassov *et al.*, Phys. Rev. D **65**, 032003 (2003).
- [49] W. M. Yao *et al.* (Particle Data Group), J. Phys. G **33**, 1 (2006).
- [50] F. Karsch, D. Kharzeev and H. Satz, Phys. Lett. B **637**, 75 (2006).
- [51] J. W. Bos, J. H. Koch and H. W. L. Naus, Phys. Rev. C **44**, 485 (1991).
- [52] M.E. Peskin and D.V. Schroeder, *An Introduction to Quantum Field Theory* (Perseus Books, Cambridge, Massachusetts, 1995).
- [53] U. Mösle, *Fields, Symmetries, and Quarks* (Springer-Verlag, Berlin Heidelberg, 1999).
- [54] J. G. Korner and M. C. Mauser, Lect. Notes Phys. **647**, 244 (2004).